Primary versus Ternary Adsorption of Proteins onto PEG Brushes

A. Halperin,*,† G. Fragneto,‡ A. Schollier,‡,§ and M. Sferrazza*,§

SPrAM/DRFMC, CEA-Grenoble, Avenue des Martyrs, F-38042 Grenoble, France, ILL, Institute Max Von Laue Paul Langevin, F-38042 Grenoble, France, and Département de Physique, Université Libre de Bruxelles, Boulevard du Triomphe, CP223, B-1050 Bruxelles, Belgium

Received April 6, 2007. In Final Form: June 8, 2007

Polyethylene glycol (PEG) brushes are used to reduce protein adsorption at surfaces. Their design needs to allow for two leading adsorption modes at the brush-coated surface. One is primary adsorption at the surface itself. The second is ternary adsorption within the brush as a result of weak PEG−protein attraction. We present a scaling theory of the equilibrium adsorption isotherms allowing for concurrent primary and ternary adsorption. The analysis concerns the weak adsorption limit when individual PEG chains do not bind proteins. It also addresses two issues of special relevance to brushes of short PEGs: the consequences of large proteins at the surface protruding out of a shallow brush and the possibility of marginal solvent conditions leading to mean-field behavior. The simple expressions for the adsorption isotherms are in semiquantitative agreement with experiments.

I. Introduction

Surfaces displaying poly(ethylene glycol) (PEG) are known for their resistance to protein adsorption. Functionalization by PEG is thus used to repress undesirable processes tractable to protein adsorption.[1−3] Examples of such negative effects include the triggering of clotting in blood-contacting devices, fouling of contact lenses, and diminished circulation time of therapeutic proteins[4] and drug-bearing liposomes.[5] The applications of functionalization by PEG span a wide range from pharmacology to food engineering. They vary with respect to the nature of the biological fluid contacting the surface and the relevant time scale. The systems also involved differ widely with respect to the nature of surface, the characteristics of the PEG, and its anchoring mode. The types of surfaces vary from rigid macroscopic surfaces of metal or plastic to soft microscopic surfaces of lipid membranes. The PEG polymers utilized include stars, linear chains, and branched polymers of different degrees of polymerization. The PEG layer can be produced by the adsorption of various types of block copolymers or by covalent grafting to the surface. A consensus concerning the optimal design of such systems is yet to emerge because of the wide scope of the problem. In part, the difficulty can be traced to unresolved questions concerning the nature of the interactions between PEG-bearing surfaces and proteins. These are evident in physical chemistry experiments concerning the interactions of brushes of terminally anchored linear PEG chains with proteins and in the theoretical models proposed to rationalize them.[6−15] As we shall elaborate shortly, three issues are involved. The first concerns the interplay of two adsorption mechanisms (Figure 1): one is primary adsorption at the surface due to surface−protein attraction, and the second is ternary adsorption within the brush as a result of weak PEG−protein attraction. A full theoretical description of the system should allow for the combined effect of the two modes. The second issue is the possibility of partial insertion of large proteins into "shallow" brushes formed by short PEG chains. In such situations, the protein can contact the surface while protruding out of the brush (Figure 1). Finally, PEG brushes in the relevant experimental range may exhibit either marginal or good solvent behavior. We address these three issues in our theoretical analysis of equilibrium protein adsorption isotherms. The theory allows for concurrent primary and ternary adsorption as well as for the possibility of partial insertion. Within our scaling approach, we consider both marginal and good solvent regimes. Importantly, the discussion of ternary adsorption invokes the weak adsorption limit. The model yields simple explicit expressions for the adsorption isotherms. In turn, these enable the fitting of experimental data and yield parameters in semiquantitative agreement with theory.

The key problem that we address concerns the mechanisms of protein adsorption onto a brush-bearing surface and their relation to the PEG's degree of polymerization, N. This is apparent upon comparison between the amount of adsorbed protein at

† CEA-Grenoble.

‡ Institute Max Von Laue Paul Langevin.

§ Université Libre de Bruxelles.

(1) Elbert, D. L.; Hubbell, J. A. *Annu. Rev. Mater. Sci.* **1996**, *26*, 365−394.
(2) Lee, H.; J.; Lee, H. B.; Andrade, J. D. *Prog. Polym. Sci* **1995**, *20*, 1043−1079.
(3) (a) Harris, J. M., Ed. *Poly(Ethylene Glycol) Chemistry: Biotechnical and Biomedical Applications*; Plenum Press: New York, 1992. (b) Harris, J. M., Zalipsky, S., Eds. *Poly(Ethylene Glycol) Chemistry and Biological Applications*; American Chemical Society: Washington, DC, 1997.
(4) Harris, J. M.; Chess, R. *Nat. Rev. Drug Discovery* **2003**, *2*, 214.
(5) Janoff, A. S., Ed. *Liposomes: Rational Design*; Marcel Dekker: New York, 1998.
(6) Halperin, A. *Langmuir* **1999**, *15*, 2525.
(7) Currie, E. P. K.; Van der Gucht, J.; Borisov, O. V.; Cohen Stuart, M. A. *Pure Appl. Chem.* **1999**, *71*, 1227−1241.
(8) Currie, E. P. K.; Norde, W.; Cohen Stuart, M. A. *Adv. Colloid Sci.* **2003**, 100−102, 205−265.
(9) Szleifer, I. *Biophys. J.* **1997**, *72*, 595.
(10) Jeon, S. I.; Lee, I.; Andrade, J. H.; de Gennes P. G. *J. Colloid Interface Sci.* **1991**, *142*, 149.
(11) Efremova, N. V.; Bondurant, B.; O'Brien, D. F.; Leckband, D. E. *Biochemistry* **2000**, *39*, 3441−3451.
(12) McPherson, T.; Kidane, A.; Szleifer, I.; Park, K. *Langmuir* **1998**, *14*, 176.
(13) Malmsten, M.; van Alstine, J. M. *J. Colloid Interface Sci.* **1996**, *177*, 502−512.
(14) Bosker, W. T. E.; Iakovlev, P. A.; Norde, W.; Cohen Stuart, M. A. *J. Colloid Interface Sci.* **2005**, *286*, 496−503.
(15) Norde, W.; Gage, D. *Langmuir* **2004**, *20*, 4162−4167.
(16) Alexander, S. *J. Phys. (Paris)* **1977**, *38*, 983.
(17) Halperin, A.; Tirrell, M.; Lodge, T. P. *Adv Polym. Sci.* **1992**, *100*, 31.
(18) Baskir, J. N.; Hatton, T. A.; Suter, U. W. *Macromolecules* **1987**, *20*, 1300−1311.
(19) Baskir, J. N.; Hatton, T. A.; Suter, U. W. *J. Phys. Chem.* **1989**, *93*, 2111−2122.
(20) Abbott, N. L.; Blankschtein, D; Hatton, T. A. *Macromolecules* **1992**, *24*, 4334−4348.
(21) Abbott, N. L.; Blankschtein, D.; Hatton, T. A. *Macromolecules* **1992**, *25*, 3917−3931.
(22) Abbott, N. L.; Blankschtein, D.; Hatton, T. A. *Macromolecules* **1992**, *25*, 3932−3941.

10.1021/la701007j CCC: $37.00
Published on Web 09/06/2007

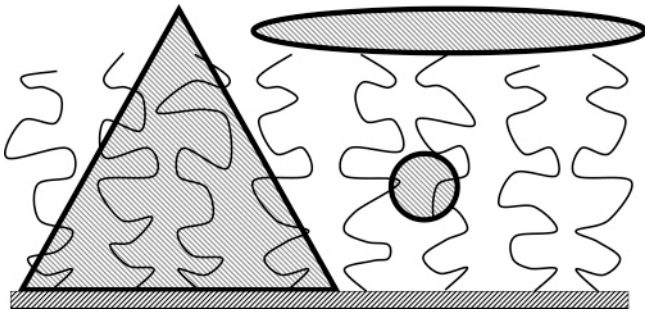

Figure 1. Protein adsorption at surfaces carrying PEG brushes may occur via three modes: (a) Primary adsorption involving an attractive contact with the surface. Here, this case is illustrated for a partially inserted protein shaped as a triangular wedge as suggested by recent models of BSA. (b) Ternary adsorption of protein within the brush itself as a result of weak PEG−protein attraction. This is illustrated for a small globular protein of spherical shape. (c) Secondary adsorption at the outer edge of the brush due to van der Waals attraction to the surface. This mode may be important for long cylindrical proteins, and it is depicted for a prolate ellipsoid.

bare surfaces and at surfaces coated by PEG brushes. For low N, $N \lesssim 150$, the brush-bearing surfaces are less adsorbing,[7,11−15] whereas for high N, $N \gg 150$, they can adsorb more than the bare surfaces.[7,14,15] In turn, existing theoretical models of these systems followed two different routes. One approach, motivated by the low-N behavior, assumes that the PEG chains do not adsorb onto proteins and their interactions are purely repulsive.[6,9,10] Within this picture, the proteins can undergo primary adsorption at the grafting surface as a result of protein−surface attraction, or secondary adsorption at the outer edge of the brush, due to van der Waals attraction between the surface and the protein (Figure 1). The second model, inspired by the high-N behavior, allows for the adsorption of PEG chains onto the protein.[7] As a result, protein ternary adsorption within the brush itself becomes possible.[7,8] Thus far, the two pictures were considered in their pure form, that is, either assuming primary and secondary adsorption occur with no ternary adsorption[6,9,10] or vice versa.[7] However, the three adsorption mechanisms may clearly operate simultaneously, thus suggesting the necessity of a unified model. The case for a unified approach is further enhanced by deficiencies in the pure-form models: (i) The low-N models predict a monotonic decrease in the mass of adsorbed protein per unit area, Γ, with the area per chain Σ. This is in agreement with low-N results but does not account for the high-N observation of a maximum in Γ at low Σ. (ii) The high-N model, proposed by Currie[7] et al., allows for numerical fits of Γ versus Σ data for both high and low N. However, this is achieved by assuming the strong adsorption of PEG onto the proteins (i.e., a long PEG chain is considered to be capable of binding a number of proteins, leading to a "pearl necklace" configuration). In turn this last assumption contradicts, as noted by the authors, experiments that show no evidence for the complexation of proteins by free PEG chains in bulk solution. Two additional issues are involved. One is the possible role of partial protein insertion as illustrated by the experiments of Bosker et al.[14] upon comparison of the protein dimensions and the brush height. To our knowledge, it has not been addressed so far. Finally, the boundary between the marginal and good solvent regimes of PEG remains to be clarified. Whereas water is a good solvent for high-N PEGs,[23−26] there are indications of mean-field (MF), marginal solvent behavior for $N \lesssim 50$.[27,28] This issue is of interest because the adsorption isotherms in the two regimes are somewhat different.

Theoretical modeling of protein−brush interactions is of interest in view of the growing number of physical chemistry-type experiments characterizing the variation of single protein Γ with Σ and N.[7,11−15] The interplay of experiment and theory affords the prospect of the rational design of brushes repressing protein adsorption. In addition, a fundamental understanding of the relative importance of primary and ternary adsorption is of immediate practical interest. Residual protein adsorption at high grafting densities is often attributed to nonhomogeneous substrate coverage permitting primary adsorption in low-coverage regions. Within the strong adsorption model of Currie et al., this effect can result from ternary protein adsorption onto the PEG chains rather than onto the surface.[7] These two views lead to radically different forecasts of the ultimate performance of PEG brushes as surface treatments for repressing protein adsorption. If brushes of short PEG adsorb proteins, then residual ternary adsorption is an inherent feature that is difficult to eliminate by technical improvement. In the opposite case, better performance may be attained by enhancing the uniformity of the coverage.

Our theoretical approach and the underlying assumptions are summarized in section II. Pure primary adsorption in a good solvent is discussed in section III. In addition, we consider partial insertion in brushes of short PEGs as illustrated by the case of bovine serum albumin (BSA) and the experiments of Norde and Gage.[15] The partial insertion scenario depends crucially on the shape of the protein. In contrast to the full insertion case, the volume and surface area of the proteins do not fully specify the free energy. Accordingly, the analysis based on the shape of BSA illustrates the necessary modifications but is not applicable to all proteins. Our subsequent discussion relies on earlier results concerning PEG−protein interactions and polymer adsorption. The necessary background is summarized in section IV and Appendix I. Pure ternary adsorption in a good solvent is considered in section V. Certain details concerning the pure scaling regimes are elaborated in Appendix II. The concurrent case, where both primary and ternary adsorption take place, is discussed in section VI. This discussion addresses the modification of primary adsorption due to PEG−protein attraction and the relative importance of primary and ternary adsorption for different values of N. The discussion in sections II and IV−VI concerns brushes immersed in good solvents. The evidence of MF behavior in solutions of short PEG is briefly summarized in section VII as well as its possible rationalization in terms of the state diagram of semiflexible chains. The combination of these two ingredients yields explicit forms for free-energy terms in the marginal solvent regime, thus specifying the necessary adaptations of the good solvent results to brushes of short chains or high grafting density. A detailed comparison between the theory and reported experimental results as well as a discussion of the difficulties involved is presented in section VIII. As noted earlier, the adsorption isotherms obtained in sections III and IV−VII apply when thermodynamic equilibrium is attained. In Appendix III, we note that results of a similar form can be obtained, in a limited range, by assuming irreversible adsorption whose rate is controlled by the passage through the brush. The kinetics corresponding to the last scenario do not agree with experiment, thus lending support to the equilibrium hypothesis.

(23) Devanand, K.; Selser, J. C. *Macromolecules* **1991**, *24*, 5943−5947.
(24) Kawaguchi, S.; Imai, G.; Suzuki, J.; Miyahara, A.; Kitano, T.; Ito, K. *Polymer* **1997**, *38*, 2885−2891.
(25) Venohr, H.; Fraaije, V.; Strunk, H.; Borchard, W. *Eur. Polym. J.* **1998**, *34*, 723−732.
(26) Wang, S.-C.; Wang, C.-K.; Chang, F.-M.; Tsao, H.-K. *Macromolecules* **2002**, 35, 9551−9555
(27) Hansen, P. L.; Cohen, J. A.; Podgornik, R.; Parsegian V. A. *Biophys. J.* **2003**, *84*, 350−355.
(28) Marsh, D. *Biophys. J.* **2004**, *86*, 2630−2633.

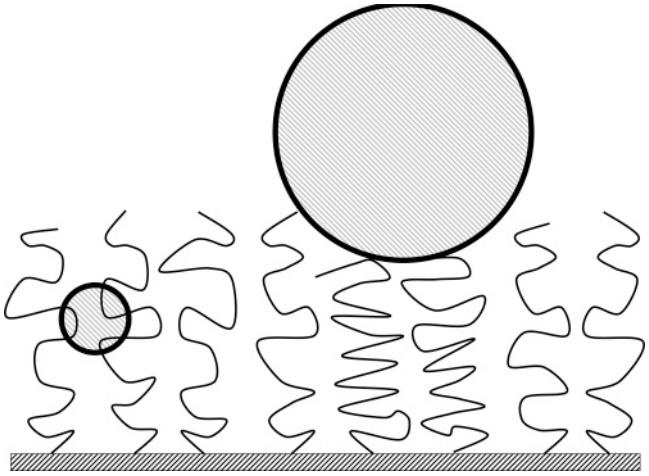

Figure 2. Adsorption of small proteins in the insertion mode does not significantly perturb the brush structure whereas large proteins can enter the brush only by inducing local compression.

II. Model

Our analysis utilizes the approach of ref 6, which allows for primary and secondary adsorption as modified to incorporate ternary adsorption. In formulating the model, we focus on the insertion mode of globular proteins into the brush. In this mode, the introduction of a protein into the brush does not perturb its overall structure. This scenario is roughly realized when two conditions are satisfied. First, the protein must be sufficiently small. Thus, for proteins of approximately spherical form, their radius R should be small compared to the brush thickness H. In the opposite limit of $R \gg H$, entry into the brush can occur only by local compression of the brush (Figure 2). Second, the surface concentration of the adsorbed proteins should be sufficiently small so that protein−protein interactions do not play a role and their behavior can be described in terms of dilute solution theory. In the following text, we consider the equilibrium adsorption isotherm of globular proteins. Because secondary adsorption is expected to play a role only for long cylindrical proteins,[6] we confine the analysis to primary and ternary adsorption. We further focus on physical chemistry experiments where the brush is immersed in a solution of a single protein species. In this case, $\Gamma \approx N_{tot}$, where $N_{tot} = N_{prim} + N_{tern}$ is the total number of adsorbed proteins per unit area reflecting the contributions of both primary and ternary adsorption, N_{prim} and N_{tern}, respectively. Because we limit the discussion to low N_{tot}, the equilibrium values of N_{prim} and N_{tern} are proportional to the concentration of free protein in the solution, c_p (i.e., $N_{prim} \approx K_{prim}c_p$ and $N_{tern} \approx K_{tern}c_p$, where K_{prim} and K_{tern} are the corresponding equilibrium constants). Altogether

$$N_{tot} \approx (K_{prim} + K_{tern})c_p \qquad (1)$$

and the relative importance of the two adsorption modes is determined by K_{prim}/K_{tern}. To simplify our discussion further, we base the analysis on the Alexander model of brushes.[16,17] In this model, the monomer concentration profile is steplike, and all chain ends straddle the upper boundary of the brush at height H. Accordingly, the monomer volume fraction in the brush is $\phi \approx Na^3/\Sigma H$, where Σ is the area per chain, a is the monomer size, and N is the degree of polymerization of the grafted chains. In a good solvent, each chain may be viewed as a fully extended string of close-packed, nonoverlapping "brush blobs" of size $\xi \approx \Sigma^{1/2}$ with each comprising $g \approx (\Sigma/a^2)^{5/6}$ monomers. The equilibrium height of an unperturbed brush is thus $H \approx (N/g)\xi \approx N(a^2/\Sigma)^{1/3}a$.

Our model incorporates three contributions to the free energy of a protein in the brush. The first two are identical to the ones introduced in ref 6, and the third is new: (i) An osmotic penalty, F_{osm}, is incurred by a protein inserted into the brush because its volume is inaccessible to the PEG monomers. For a fully inserted protein of volume $V_{protein}$, it is $F_{osm} = \pi V_{protein}$ where π is the osmotic pressure in the brush. This penalty opposes both primary and ternary adsorption. (ii) Primary adsorption is driven by surface−protein attraction as characterized by the adsorption free energy of a protein at the surface, U_{ads}. (iii) Ternary adsorption is due to PEG−protein attraction of $-\epsilon kT$ per monomer in contact with the protein, where k denotes the Boltzmann constant and T is the temperature. In the weak adsorption limit, we consider small ϵ such that individual PEG chains do not bind proteins but ternary adsorption nevertheless occurs because an inserted protein experiences attractive contacts with several chains. The corresponding adsorption free energy, F_{ads}, is determined by the number of protein−monomer contacts. In turn, this depends on the surface area of the protein, $A_{protein}$, and the monomer concentration, $c \approx (a^2/\Sigma)^{2/3}$. Three features of F_{ads} merit comment. First, in distinction to Currie et al.,[7] F_{ads} varies with $A_{protein}$, ϵ, and Σ. Second, ternary adsorption occurs only in the brush regime and does not contribute to Γ of the mushroom range. Our description thus follows, in spirit, the approach of Baskir et al. and Abbott et al.[18−22] rather than the one adopted by Currie et al. Finally, proteins at the surface also experience attractive PEG contacts. Accordingly, F_{ads} is involved in both primary and ternary adsorption. The three free-energy terms discussed above contribute to protein−brush interactions for all N. However, the precise forms of F_{osm} and F_{ads} may assume somewhat different forms for brushes of low and high N. Two effects are involved: First, large proteins at the surface may protrude out of a brush formed by low-N chains, and this requires a modification of $V_{protein}$ and $A_{protein}$. Second, low-N brushes attain higher grafting densities where marginal solvent, MF behavior is expected to replace good solvent scaling. In turn, MF behavior affects both F_{osm} and F_{ads} and, as a result, the adsorption isotherms.

For simplicity, most of our discussion utilizes the good solvent blob picture where the free energies involved acquire a compact, transparent form. It is important to clarify our handling of the two types of numerical factors playing a role in the problem. One group is associated with the shape of the proteins. These appear, for example, in $V_{protein}$ and $A_{protein}$. The second, which is the polymer group, comprises unknown numerical prefactors in π and F_{ads}. Our analysis incorporates explicitly only the geometrical numerical prefactors. This is justified because we consider effects traceable to protein shape and dimensions while the unknown polymer factors remain constant.

III. Pure Primary Adsorption: Full versus Partial Insertion in a Good Solvent

First, it is helpful to consider the pure primary adsorption of proteins whose interactions with PEG are fully repulsive (i.e., the adsorption free energy of a PEG monomer at the surface of the protein is $-\epsilon kT = 0$ [6]). In this case, a protein in contact with the bare surface gains an adsorption free energy U_{ads} measured with respect to its free energy in the bulk solution. When the protein is fully inserted into the brush, the osmotic penalty incurred by the protein is $F_{osm} \approx V_{protein}\pi$ where $V_{protein}$ is the volume of the protein and $\pi \approx kT/\xi^3$ is the local osmotic pressure in the brush. This estimate is justified when the protein dimensions are large in comparison to ξ. Within the Alexander model we utilize F_{osm} is constant throughout the layer

$$\frac{F_{\rm osm}}{kT} \approx \frac{V_{\rm protein}}{\Sigma^{3/2}} \tag{2}$$

Accordingly, the free energy of a protein undergoing primary adsorption at the interface is $F_{\rm prim} = U_{\rm ads} + F_{\rm osm}$.

$$F_{\rm prim} \approx U_{\rm ads} + kT\frac{V_{\rm protein}}{\Sigma^{3/2}} \tag{3}$$

The fraction of occupied surface sites is $\theta = N_{\rm prim}/N_{\rm prim}^{\rm max}$, where $N_{\rm prim}^{\rm max}$ is the saturation value of $N_{\rm prim}$. When the surface excess of proteins is low, the fraction of surface sites occupied by adsorbed proteins is small, $\theta \ll 1$, and the chemical potential of proteins at the surface is $\mu_{\rm prim} \approx U_{\rm ads} + kTV_{\rm protein}/\Sigma^{3/2} + kT \ln \theta$. The chemical potential of the free proteins is $\mu_{\rm bulk} \approx kT \ln c_{\rm p}$, where $c_{\rm p}$ is the dimensionless number concentration of proteins in the solution.[29] The equilibrium condition $\mu_{\rm prim} = \mu_{\rm bulk}$ yields $N_{\rm prim} \approx K_{\rm prim}c_{\rm p}$, where $K_{\rm prim} \approx N_{\rm prim}^{\rm max} \exp(-F_{\rm prim}/kT)$. The primary adsorption is thus essentially repressed when $F_{\rm prim} \approx 0$ is attained at

$$\Sigma_{\rm co}^{\rm prim} \approx \left(\frac{kTV_{\rm protein}}{|U_{\rm ads}|}\right)^{2/3} \tag{4}$$

Significant primary adsorption is thus expected in the range of $\infty > \Sigma > \Sigma_{\rm co}^{\rm prim}$ though eq 4 is applicable only in the brush regime, $\Sigma < R_{\rm F}^2$.

The adsorption and desorption behavior of proteins typically exhibits hysteresis, and $U_{\rm ads}$ values are thus difficult to establish. Theoretical estimates of $U_{\rm ads}$ vary over a wide range and depend strongly on the protein and the surface.[30] In addition, $U_{\rm ads}$ may be modified by the PEG brush. For example, the brush may counter structural rearrangements following adsorption that contribute to $U_{\rm ads}$ at the bare surface. Accordingly, it is difficult to estimate the absolute values of $K_{\rm prim}$. It is, however, possible to study its Σ dependence. For comparison with experimental data, it is convenient to express $N_{\rm prim} \approx K_{\rm prim}c_{\rm p}$ in the form

$$\ln N_{\rm prim} \approx {\rm const}' - \frac{V_{\rm protein}}{\sum^{3/2}} \tag{5}$$

where ${\rm const}' \approx -U_{\rm ads}/kT + \ln c_{\rm protein} + \ln N_{\rm prim}^{\rm max}$. We will demonstrate the utility of this form in section VIII.

The full insertion condition is easily satisfied for brushes of long PEG chains. In the opposite limit, it is necessary to allow for the possibility of partial insertion with part of the protein protruding out of the brush. The analysis of this situation depends strongly on the shape and dimensions of the protein. To illustrate this point, we consider the case of bovine serum albumin (BSA). Two models of BSA were invoked in the descriptions of adsorption experiments. BSA has been traditionally described as a "cigar-like" prolate ellipsoid with minor semiaxes of length 20 Å and a major semiaxis of length 70 Å.[31] However, recent evidence suggests a "heart-shaped" structure approximated as an equilateral triangular wedge with edges of length 80 Å and thickness of 30 Å.[32] When the cigar-like shape is assumed, the BSA can adsorb onto the surface with its major axis parallel to the surface. For relatively thin brushes, with $H \approx 50$ Å, full immersion in the insertion mode is possible in view of the small length of the minor semiaxes. The situation is different for the heart-shaped model. In this case, the insertion mode can be realized if the BSA adsorbs with its narrow edge at the surface. Within this model, the height of the triangle, $h = 80\sqrt{3}/2$ Å ≈ 70 Å can exceed the height H of a thin brush. The protruding part is an equilateral triangular wedge of height $h_{\rm out} = h - H$, and the volume of the protein immersed in the brush is then $V_{\rm in} = V_{\rm p}[1 - (h_{\rm out}/h)^2] = (V_{\rm p}H/h)(2 - H/h)$. The osmotic penalty $\pi V_{\rm in}$ corresponding to partial insertion is thus smaller and exhibits both N and Σ dependencies. The signatures of this effect vary with the experimental design. For example, in the experiment of Bosker et al. Γ of BSA is measured for different Σ and constant N.[14] In this case, it is convenient to express the partial insertion penalty $F_{\rm osm}^{\rm p}(\Sigma)$ in terms of Σ_h, as introduced via $h/a \approx N(a^2/\Sigma_h)^{1/3}$, leading to

$$\frac{F_{\rm osm}^{\rm p}(\Sigma)}{kT} \approx \frac{V_{\rm protein}\Sigma_h^{1/3}}{\Sigma^{11/6}}\left[2 - \left(\frac{\Sigma_h}{\Sigma}\right)^{1/3}\right] \qquad \Sigma \geq \Sigma_h, N = {\rm const}' \tag{6}$$

and

$$N_{\rm prim}^{\rm p}(\Sigma) \approx N_{\rm prim}^{\rm max}c_{\rm p}\exp\left\{\frac{|U_{\rm ads}|}{kT} - \frac{V_{\rm protein}\Sigma_h^{1/3}}{\Sigma^{11/6}}\left[2 - \left(\frac{\Sigma_h}{\Sigma}\right)^{1/3}\right]\right\} \qquad \Sigma \geq \Sigma_h, N = {\rm const}' \tag{7}$$

In contrast, in the experiment of Norde and Gage[15] the signatures of this effect are visible in the N dependence of Γ for constant Σ. Accordingly, it is convenient to introduce N_h corresponding to $H = h$ via $h/a \approx N_h(a^2/\Sigma)^{1/3}$, thus leading to a partial insertion penalty of

$$\frac{F_{\rm osm}^{\rm p}(N)}{kT} \approx \frac{V_{\rm protein}}{\Sigma^{3/2}}\frac{N}{N_h}\left(2 - \frac{N}{N_h}\right) \qquad N \leq N_h, \Sigma = {\rm const}' \tag{8}$$

and to

$$N_{\rm prim}^{\rm p}(N) \approx N_{\rm prim}^{\rm max}c_{\rm p}\exp\left[\frac{|U_{\rm ads}|}{kT} - \frac{V_{\rm protein}}{\Sigma^{3/2}}\frac{N}{N_h}\left(2 - \frac{N}{N_h}\right)\right] \qquad N \leq N_h, \Sigma = {\rm const}' \tag{9}$$

In qualitative agreement with the experimental results, $\Gamma \approx N_{\rm prim}$ decreases with N in the range of $N \leq N_h$ (Figure 3). It is useful to note two differences between the $N = {\rm const}'$ and $\Sigma = {\rm const}'$ experiments: (i) In $N = {\rm const}'$ experiments, the variation in Σ affects both $H/a \approx N(a^2/\Sigma)^{1/3}$ and $\pi \approx kT/\Sigma^{3/2}$, whereas in $\Sigma = {\rm const}'$ experiments, only H is modified. (ii) Clearly H is more sensitive to variation in N. Increasing Σ by 10 results in a roughly 2-fold decrease in H. Altogether, $N = {\rm const}'$ experiments thus lead to clearer signatures of partial insertion.

IV. Protein−PEG Interactions and Weak Polymer Adsorption: A Reminder

As noted earlier, $-\epsilon kT < 0$ modifies the primary adsorption at the surface and gives rise to ternary adsorption within the brush. Before we consider these two effects, it is helpful to provide the background on ϵ of proteins and to summarize some results concerning the adsorption of polymers at surfaces. The available information on the interaction free energy between PEG monomers and protein surfaces, $-\epsilon kT$, is actually limited. An analysis of experiments on the partitioning of certain proteins between two coexisting phases suggests that the interactions

(29) The chemical potential of the free proteins is $\mu_{\rm bulk} = kT \ln a_{\rm p}$ where $a_{\rm p} = \gamma c_{\rm p}$ is the dimensionless activity and γ is the activity coeffcient. $\gamma \rightarrow 1$ as $c_{\rm p} \rightarrow 0$,[59] and for simplicity, we thus utlize $c_{\rm p}$ instead of $a_{\rm p}$.

(30) Norde, W. In *Physical Chemistry of Biological Interfaces*; Baszkin, A., Norde, W., Eds.; Marcel Dekker: New York, 2000.

(31) Squire, P. G.; Moser, P.; O'Konski, C. T. *Biochem. J.* **1968**, *7*, 426.

(32) Carter, D. C.; Ho, J. X. *Adv. Protein Chem.* **1994**, *45*, 153.

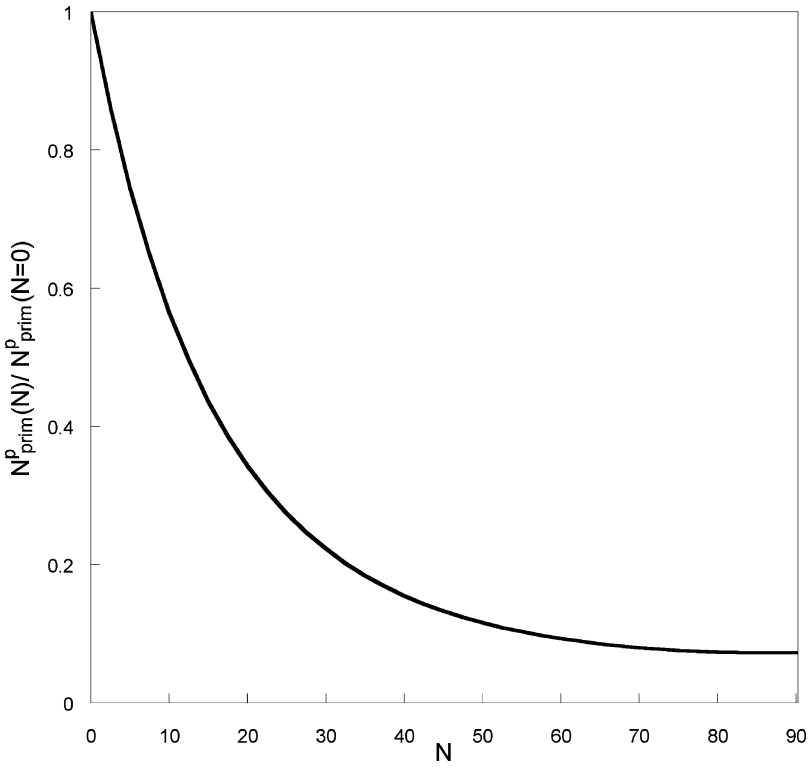

Figure 3. Partial insertion is associated with a decrease in $\Gamma(N)$ upon increasing N for $N \leq N_h$ at constant Σ as seen from the plot of $N^{p}_{prim}(N)/N^{p}_{prim}(N=0)$ vs N utilizing eq 9 with $V_{protein} = 8.3 \times 10^4$ Å^3 for "triangular" BSA and $\Sigma = 1000$ Å^2 utilized by Norde and Gage.[15]

between the PEG monomers and the proteins are weakly attractive.[18−22] A theoretical study of such experiments indicated ϵ values varying in the range of 0.1−0.01.[21] An analysis of small-angle neutron scattering (SANS) experiments on BSA in PEG solutions led to $\epsilon = 0.05$.[22] It is useful to note two reservations concerning these results. First, the ϵ values cited above are model-dependent, and three related issue are of special importance for our subsequent discussion: (i) the protein surface was assumed to be uniform; (ii) the PEG polymer was modeled as a homopolymer comprising a single type of monomer; and (iii) the results depend on the assumed shape of the protein. For example, in the analysis of the SANS experiment, BSA was considered to be a prolate ellipsoid,[31] although subsequent structural studies suggest a heart-like platelet shape.[32] This last point is significant because the surface area of the protein is an important parameter in this problem. Second, for practical reasons the ϵ values were obtained only for a small number of proteins. Accordingly, the range of ϵ remains to be established. At this junction, it is of interest to recall the analogy, noted by a number of authors,[7,21] between the protein−PEG system and ternary aqueous solutions of PEG and micelles of low-molecular-weight amphiphiles. Importantly, PEG adsorbs onto anionic micelles while the attraction to cationic and nonionic micelles is weaker or absent altogether. Because the charge and hydrophobicity of protein surfaces vary over a wide range, this analogy suggests that $\epsilon = 0$ may occur for certain proteins. At the same time, the absence of reports of complexation of proteins by PEG chains in aqueous solutions suggests $\epsilon \ll 1$. With these reservation in mind, we will assume, for lack of better data, that $\epsilon = 0.05$ is a typical value.

The adsorption free energy of a protein inserted into a PEG brush is determined by ϵ and the number of monomers in contact with the protein. To estimate the number of such contacts, it is first useful to recall exact results concerning the behavior of a self-avoiding random walk (SAW) at grazing contact with a weakly adsorbing planar surface (Appendix I). This case corresponds to a flexible chain in an athermal good solvent. The number of monomers in contact with the surface is N^{Φ}, where N is the degree of polymerization and $\Phi \approx {}^3/_5$ is the exponent describing the crossover from nonadsorbed to adsorbed configurations. The condition $N^{\Phi}\epsilon \approx 1$ or $\epsilon_c \approx N^{-3/5}$ defines the adsorption threshold for such a chain. When $\epsilon \ll \epsilon_c$, the adsorption free energy of the chain is much lower than kT, and the chain configuration is unperturbed. For $\epsilon \gg \epsilon_c$, the chain configurations are strongly modified. In particular, a single chain at the surface will form a 2D SAW of adsorption blobs,[33] with each comprising g_{ad} monomers such that $g_{ad}^{\Phi}\epsilon \approx 1$ and the blob size $\xi_{ad} \approx g_{ad}^{3/5}a$ is

$$\xi_{ad} \approx \frac{a}{\epsilon} \tag{10}$$

and

$$g_{ad} \approx \epsilon^{-5/3} \tag{11}$$

Because each adsorption blob contributes an adsorption free energy of kT, long chains with $N \gg g_{ad}$ experience an adsorption free energy of $(N/g_{ad})kT \gg kT$. The adsorption threshold $N^{\Phi}\epsilon \approx 1$ thus involves two signatures. One concerns the configuration of a single adsorbed chain, and the second pertains to the amount of adsorbed polymer upon immersing the surface in a dilute solution of mobile polymers. In particular, when $N \gg g_{ad}$ surface saturation follows equilibration with a dilute polymer solution. For a planar surface immersed in a dilute polymer solution, weak adsorption is thus defined by the condition $N < g_{ad}$ or, equivalently, $R_F < \xi_{ad}$. In the case of a surface in contact with a semidilute solution with a blob size ξ, the weak adsorption

(33) Bouchaud, E.; Daoud, M. *J. Phys (Paris)* **1987**, *48*, 1991−2000 and refrences cited therein.

condition becomes $\xi < \xi_{ad}$. This picture is modified when small colloidal particles replace the planar surface.[34−39] One important difference concerns the adsorption threshold. In the planar case, each monomer in the chain can adsorb, and thus $\epsilon_c \approx N^{-3/5} \rightarrow 0$ as $N \rightarrow \infty$. In contrast, the surface area of a small particle limits the number of monomers that can adsorb. As a result, the adsorption threshold occurs at a finite ϵ_c even in the limit of $N \rightarrow \infty$. For a spherical particle of radius R, a lower bound of ϵ_c is given by $(R/a)^2\epsilon \approx 1$,[35] and computer simulations indeed show that ϵ_c increases as the particle diminishes in size.[40] For future discussions, we emphasize that the results summarized above are applicable as long as the particle is large in comparison to ξ_{ad} or to the blob size of the polymer solution, ξ. Discussions of polymer adsorption onto colloidal particles typically focused on the strong adsorption limit.[34,35,39,41] They addressed the structure of the adsorbed layer and the aggregation behavior induced by polymer adsorption onto the particles (i.e., gelation due to the adsorption of a number of chains onto each particle vs the pearl necklace configuration where each chain adsorbs a number of particles). As we shall argue below, the opposite limit applies to proteins within PEG brushes.

The onset of adsorption of a flexible chain at an infinite planar surface with $\epsilon = 0.05$ occurs at $N \approx 150$ and involves $N_c \approx N^{3/5} \approx 20$ monomers in contact with the surface. For PEG, when modeled as a flexible chain with $a = 3.5$ Å the adsorption blob size is $\xi_{ad} \approx {}^{a}/_{\epsilon} = 70$ Å. As we discussed, for a small colloidal particle the number of monomers at the surface may be smaller than N_c, thus preventing the attainment of the adsorption threshold at $\epsilon = 0.05$. This suggests that PEG chains of $N \leq 150$ do not adsorb onto proteins and that ϵ values higher than $\epsilon = 0.05$ may well be required to induce such adsorption. However, the adsorption of proteins within a PEG brush does not necessarily involve a strong adsorption of individual PEG chain onto the proteins. As we shall discuss, the insertion of a protein into the brush gives rise to sufficient number of attractive contacts even though it does not involve strong adsorption and does not induce configurational changes in the brush chains (i.e., it does not modify the brush blobs to adsorption blobs). The ternary adsorption via this mechanism is actually similar to the partitioning of proteins between two coexisting "phases", the aqueous solution and the brush. For simplicity, we first consider pure ternary adsorption for PEG brushes grafted onto nonadsorbing surfaces, $U_{ads} = 0$. We will later discuss, in section VI, the case of ternary adsorption at surfaces that do adsorb, $U_{ads} < 0$.

V. Pure Ternary Adsorption in a Good Solvent

Having discussed pure primary adsorption at the surface, $U_{ads} < 0$ and $\epsilon = 0$, we now turn to the case of pure ternary adsorption within the brush, $U_{ads} = 0$ and $\epsilon < 0$. Attraction to the protein surface does not affect the blob structure as long as the brush blobs are small compared to the adsorption blobs[33] (i.e., $\xi \approx \Sigma^{1/2} < \xi_{ad}$). For $\xi_{ad} \approx 70$ Å, this implies that $\Sigma \lesssim 5000$ Å^2. In this regime, a fully inserted protein with surface area $A_{protein}$ is in contact with $A_{protein}/\xi^2$ brush blobs. In turn, each one of these blobs contributes g^{Φ} monomer−protein contacts. The overall adsorption free energy of an inserted protein is thus $F_{ads}/kT \approx -(A_{protein}/\xi^2)g^{\Phi}\epsilon$ or (Appendix I)

$$\frac{F_{ads}}{kT} \approx -\frac{A_{protein}\epsilon}{\Sigma^{1/2}a} \approx \frac{A_{protein}}{\Sigma^{1/2}\xi_{ad}} \approx -\left(\frac{\Sigma_{ads}}{\Sigma}\right)^{1/2} \quad (12)$$

where Σ_{ads} is defined by the condition $F_{ads} \approx -kT$ or

$$\Sigma_{ads} \approx \frac{A_{protein}^{\ 2}}{\xi_{ad}^{\ 2}} \quad (13)$$

Σ_{ads} roughly defines the adsorption threshold for fully inserted proteins because $F_{ads} < -kT$ when $\Sigma < \Sigma_{ads}$. The adsorption free energy is opposed by the osmotic penalty (eq 2). The two terms balance each other, $F_{osm} \approx |F_{ads}|$, at

$$\Sigma_{co}^{tern} \approx \frac{V_{protein}\xi_{ad}}{A_{protein}} \quad (14)$$

and the osmotic penalty essentially represses ternary adsorption for $\Sigma < \Sigma_{co}^{tern}$. Accordingly, $F_{osm}/|F_{ads}| \approx \Sigma_{co}^{tern}/\Sigma$, and the free energy of a protein undergoing ternary adsorption within the brush, $F_{tern} = F_{ads} + F_{osm}$, is

$$\frac{F_{tern}}{kT} \approx -\frac{A_{protein}}{\Sigma^{1/2}\xi_{ad}} + \frac{V_{protein}}{\Sigma^{3/2}} \approx \left(\frac{\Sigma_{ads}}{\Sigma}\right)^{1/2}\left(\frac{\Sigma_{co}^{tern}}{\Sigma} - 1\right) \quad (15)$$

When the concentration of proteins in the brush is low, their chemical potential is $\mu_{tern} \approx F_{tern} + kT \ln c_{tern}$, where $c_{tern} \approx N_{tern}/H \approx N_{tern}/Na\ (\Sigma/a^2)^{1/3}$, N_{tern} is the number of proteins per unit area undergoing ternary adsorption within the brush, and c_{tern} is thus the corresponding number concentration.[29] The adsorption isotherm, as obtained by equating μ_{tern} and $\mu_{bulk} \approx kT \ln c_p$, is

$$N_{tern} = K_{tern}c_p \approx c_p Na\left(\frac{a^2}{\Sigma}\right)^{1/3} \exp\left[\left(\frac{\Sigma_{ads}}{\Sigma}\right)^{1/2}\left(1 - \frac{\Sigma_{co}^{tern}}{\Sigma}\right)\right] \quad (16)$$

Two aspects of K_{tern} merit comment. The first concerns the pre-exponential factor in K_{tern} that is the counterpart of N_{prim}^{max} in K_{prim}. However, in contrast to N_{prim}^{max} this factor varies with N and Σ. This difference is due to the entropy of the adsorbed proteins. Primary adsorption occurs at the planar surface and is associated with the mixing entropy of a 2D solution. Ternary adsorption takes place within a layer of finite thickness H, and the relevant mixing entropy assumes the form $S \approx kN_{tern}\ln(eH/N_{tern})$. Because of the N dependence of this pre-exponential factor, ternary adsorption dominates primary adsorption for brushes comprising long chains. The second feature is that K_{tern}

$$K_{tern} = \frac{H_{ads}}{a}y^{1/3}\exp[y^{1/2}(1 - \alpha y)] \equiv \frac{H_{ads}}{a}f(y) \quad (17)$$

exhibits a maximum at Σ_{max} in contrast to the monotonically decreasing $K_{prim}(\Sigma)$ (Figure 4). Here, $H_{ads}/a = N(a^2/\Sigma_{ads})^{1/3}$ is the brush height at $\Sigma = \Sigma_{ads}$, $y = \Sigma_{ads}/\Sigma$, and $\alpha = \Sigma_{co}^{tern}/\Sigma_{ads}$. Equation 17 is applicable for brushes that are not too dense when $\Sigma_{ads}/a^2 \gg y \gg \Sigma_{ads}/R_F^2$. The extremum condition $\partial f/\partial y = 0$ specifies a maximum at y_{max} given by

$$\frac{1}{3} + \frac{1}{2}y_{max}^{1/2} = \frac{3}{2}\alpha y_{max}^{3/2} \quad (18)$$

Simple expressions for y_{max} and Σ_{max} are obtainable in the limits

(34) Alexander, S. *J. Phys. (Paris)* **1977**, *38*, 977.
(35) Pincus, P. A.; Sandroff, C. J.; Witten, T. A. *J. Phys. (Paris)* **1984**, *45*, 725.
(36) Marques, C. M.; Joanny, J. F. *J. Phys. (Paris)* **1988**, *49*, 1103−1109.
(37) Birshtein, T. M.; Borisov O. V. *Polymer* **1991**, *32*, 916. Birshtein, T. M.; Borisov O. V. *Polymer* **1991**, *32*, 923.
(38) Eisenriegler, E.; Hanke, A.; Dietrich, S. *Phys. Rev. E* **1996**, *54*, 1134.
(39) Aubouy, M.; Raphael, E. *Macromolecules* **1998**, *31*, 4357−4363.
(40) Nowicki, W. *Macromolecules* **2002**, *35*, 1424−1436.
(41) Johner, A.; Joanny, J. F.; Diez Orrite, S.; Bonet-Avalos, A. *Europhys. Lett.* **2001**, *56*, 549.

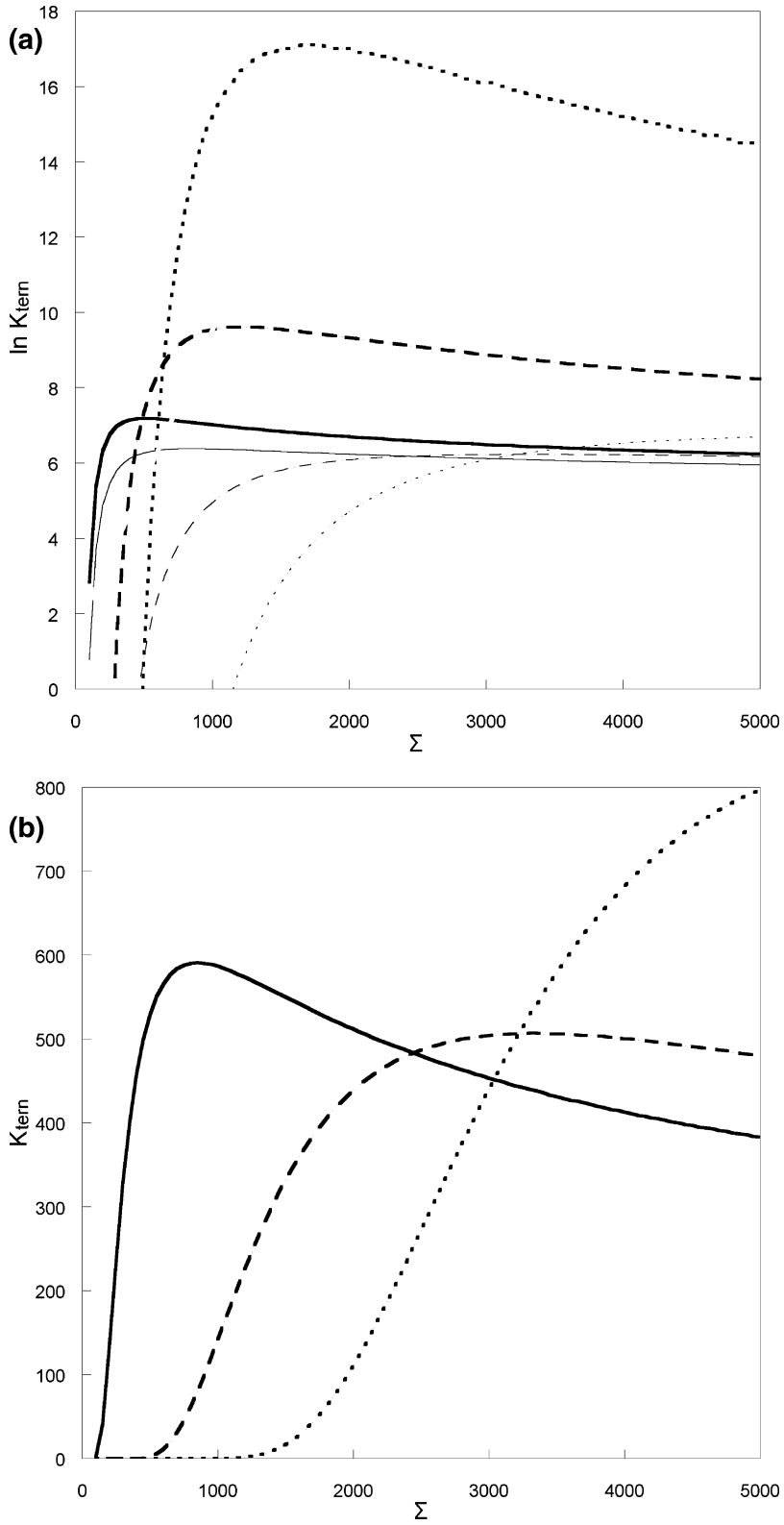

Figure 4. (a) Plot of $K_{tern}(\Sigma)$ as given by eq 17 within the brush range of PEG $N = 770$ for unimeric BPTI (−), BSA triangle (---) and anhydrous fibrinogen (− · −) assuming $\epsilon = 0.05$; the lower three curves in gray depict the corresponding results for $\epsilon = 0.01$. (b) Plot of $K_{tern}(\Sigma)$ for the same systems with $\epsilon = 0.01$.

of $y_{max} \ll 1$ and $y_{max} \gg 1$. When $y_{max} \approx {}^1/_3\alpha \gg 1$, the maximum at

$$\Sigma_{max} \approx 3\Sigma_{co}^{tern} \tag{19}$$

corresponds to the case of $\Sigma_{ads} \gg \Sigma_{co}^{tern}$, and thus $\Sigma_{ads} \gg \Sigma_{max} > \Sigma_{co}^{tern}$. In this $\alpha \ll 1$ limit, K_{tern} exhibits a pronounced maximum of $f(y_{max}) \approx \alpha^{-1/3} \exp[{}^2/_3({}^1/_3\alpha)^{1/2}] \gg 1$. In the opposite limit, of $y_{max} \ll 1$ corresponding to $\alpha \gg 1$ or $\Sigma_{ads} \ll \Sigma_{co}^{tern}$, a shallow maximum occurs at

$$\Sigma_{max} \approx \Sigma_{ads}\left(\frac{\Sigma_{co}^{tern}}{\Sigma_{ads}}\right)^{2/3} \gg \Sigma_{ads} \tag{20}$$

where $f(y_{max}) \approx \alpha^{-2/9} \ll 1$. Because the behavior of K_{tern} is

largely determined by α, it is important to note that $\alpha \approx V_{protein}\xi_{ad}^3/A_{protein}^3$ is rather sensitive to $\xi_{ad} \approx {}^a/_\epsilon$ (Figure 4). For roughly spherical proteins of radius R

$$\alpha \approx \frac{1}{3(4\pi)^2}\left(\frac{\xi_{ad}}{R}\right)^3 \qquad (21)$$

Accordingly, $\alpha \ll 1$ when $\epsilon = 0.05$ and $\xi_{ad} = 70$ Å, but $\alpha \gg 1$ may well occur for $\epsilon = 0.01$ and $\xi_{ad} = 350$ Å.

As opposed to primary adsorption, ternary adsorption involves the brush rather than the surface itself. While primary adsorption occurs on a bare surface, ternary adsorption occurs only at brush-coated surfaces. Significant ternary adsorption occurs when $F_{tern} < -kT$ and the exponential factor in eq 16 is large. This requires $\Sigma > \Sigma_{co}^{tern}$ on one hand and $\Sigma < \Sigma_{ads}$ on the other. It is thus possible to distinguish between a number of scenarios: There is only weak ternary adsorption when $\Sigma_{ads} \le \Sigma_{co}^{tern}$ (i.e., the osmotic penalty exceeds the adsorption free energy for all Σ in the brush regime). In the opposite case of $\Sigma_{ads} > \Sigma_{co}^{tern}$, it is necessary to take into account the maximal possible size of a brush blob, $\approx R_F$, as it occurs at the onset of chain overlap. When $\Sigma_{ads} > \Sigma_{co}^{tern} > R_F^2$, the adsorption regime cannot be attained because it involves unrealizable brushes for the N that is utilized. For $\Sigma_{ads} > R_F^2 > \Sigma_{co}^{tern}$, adsorption will occur at low grafting densities but will be repressed at higher grafting densities with $\Sigma < \Sigma_{co}^{tern}$. Finally, for $R_F^2 > \Sigma_{ads} > \Sigma_{co}^{tern}$ we may expect a reentrant behavior as the grafting density increases: Essentially no adsorption occurs between the overlap threshold and Σ_{ads} when $F_{ads} < kT$. Adsorption occurs at intermediate densities $\Sigma_{ads} > \Sigma > \Sigma_{co}^{tern}$ and it is repressed again at high densities when $\Sigma < \Sigma_{co}^{tern}$. N_{tern} exhibits a pronounced maximum at $\Sigma_{max} \approx 3\Sigma_{co}^{tern}$ that is, however, observable only when $\Sigma_{max} < R_F^2$.

Within our model, the boundaries of the ternary adsorption regime Σ_{ads} and Σ_{co}^{tern} are determined by the shape and the dimensions of the proteins as reflected in $V_{protein}$ and $A_{protein}$ and by the attraction energy $-\epsilon kT$. A "pure" scaling analysis, ignoring all numerical factors, indicates that ternary adsorption is possible only for highly nonspherical proteins (Appendix II). As noted is section II, our analysis incorporates the numerical prefactors in $V_{protein}$ and $A_{protein}$, thus permitting ternary adsorption for a wider class of proteins. To illustrate the effect of $V_{protein}$ and $A_{protein}$, we consider three examples: bovine pancreatic trypsin inhibitor (BPTI), BSA, and fibrinogen. We specify below their rough shape, dimensions, and the corresponding $V_{protein}$ and $A_{protein}$. BPTI is a small protein modeled as a prolate ellipsoid with minor semiaxes of length 10.5 Å and a major semiaxis of length 15 Å.[11] Two models of BSA are invoked in the literature: An early model within which BSA is described as a prolate ellipsoid with minor semiaxes of length 20 Å and a major semiaxis of length 70 Å.[31] The second, more recent model involves a heart-shaped structure approximated as an equilateral triangular wedge with edges of length 80 Å and thickness 30 Å.[32] Early electron microscopy images of fibrinogen led to a trinodular model involving three equidistant spherical domains joined by narrow cylinders.[42] Its physical properties, allowing for its anhydrous volume, suggest a cylinder of length 450 Å and a radius of 17 Å.[43] Recent studies of the hydrated fibrinogen suggest a thicker cylindrical protein with length 450 Å and radius 45 Å.[44] The corresponding $V_{protein}$ and $A_{protein}$ are summarized in Table 1.[45]

Table 1

protein	$V_{protein}$ (Å^3)	$A_{protein}$ (Å^2)
BPTI unimer	6.93×10^3	1.79×10^3
BSA (ellipsoid)	1.18×10^5	1.43×10^4
BSA (triangle)	8.3×10^4	1.27×10^4
fibrinogen (anhydrous)	4.08×10^5	4.8×10^4
fibrinogen (hydrated)	2.86×10^6	1.27×10^5

Table 2

protein	Σ_{ads} (Å^2)	Σ_{co}^{tern} (Å^2)	α	Σ_{max} (Å^2)
BPTI unimer	6.5×10^2	2.71×10^2	4.17×10^{-1}	4×10^2
BSA (ellipsoid)	4.0×10^4	6.0×10^2	1.5×10^{-2}	1.44×10^3
BSA (triangle)	3.2×10^4	4.57×10^2	1.43×10^{-2}	1.1×10^3
fibrinogen (anhydrous)	4.7×10^5	5.95×10^2	1.27×10^{-3}	1.72×10^3
fibrinogen (hydrated)	3.27×10^6	1.58×10^3	4.83×10^{-4}	4.52×10^3

As illustrated by the cases of BSA and fibrinogen, the accepted models can change with time and may be a subject of debate. The BPTI values correspond to a unimer. Note, however, the possibility of BPTI self-association leading to the formation of decamers.[46] Assuming $\epsilon = -0.05$ and thus $\xi_{ad} = 70$ Å leads to Σ_{ads}, Σ_{co}^{tern}, α, and Σ_{max} values as summarized in Table 2.

Note that the calculated Σ_{ads} values of fibrinogen occur at $\Sigma > 5000$ Å^2 and thus imply $\xi > \xi_{ad}$. These values should be considered with caution because they occur outside the applicability regime of our treatment. As illustrated by Table 2, the different $V_{protein}$ and $A_{protein}$ translate into a wide variation in the ternary adsorption regime, $\Sigma_{ads} > \Sigma > \Sigma_{co}^{tern}$ (Figure 4). The experimental accessibility of the $\Sigma_{ads} > \Sigma > \Sigma_{co}^{tern}$ range is largely determined by N. For example, for $N = 770$ utilized by Bosker et al.,[14] $R_F \approx N^{3/5}a \approx 190$ Å and the onset of the brush regime occurs roughly at $R_F^2 \approx 3.6 \times 10^4$ Å^2. Accordingly, brushes with $N > 770$ are needed in order to observe the full ternary adsorption range of fibrinogen. Brushes with $N = 770$ pose a different problem for experiments involving unimeric BPTI. In this case, the low Σ of the ternary adsorption range gives rise to a high brush penalty, $N(a^2/\Sigma)^{5/6}kT$ per PEG chain. In turn, this may hamper the fabrication of the brush, thus suggesting the use of shorter PEG polymers.

VI. Concurrent Primary and Ternary Adsorption

Our preceding discussion requires two modifications when the proteins encounter both $U_{ads} < 0$ and $\epsilon < 0$. The first concerns the primary adsorption itself because a protein at the surface will experience attractive monomer−protein contacts in addition to U_{ads}. The second is that Γ now reflects both primary and ternary adsorption and their relative importance is determined by K_{prim}/K_{tern}.

The first effect requires an adaptation of F_{prim}. In particular, F_{prim} as specified by eq 3 should be supplemented by a term reflecting for the attractive interactions with the surrounding PEG chains. For the full insertion case, the preceding discussion of ternary adsorption suggests the form

(42) Hall, C. E.; Slayter, H. S. *J. Biophys. Biochem. Cytol.* **1959**, *5*, 11−17.
(43) Knoll, D.; Hantgan, R.; Williams, J.; McDonagh, J.; Hermans, J. *Biochemistry* **1984**, *23*, 3708−3715.
(44) Bachmann, L.; Schmitt-Fumain, W. W.; Hammel, R.; Lederer, K., *Makromol. Chem.* **2003**, *176*, 2603−2618.
(45) The volume V_p and area A_p of a prolate ellipsoid with major semiaxis c and two equal minor minor axes a are $V_p = {}^4/_3\pi ca^2$ and $A_p = 2\pi a^2 + 2\pi^{ac}/_e \sin^{-1} e$ where $e = (\sqrt{c^2-a^2})/c$. Beyer, W. H. *CRC Standard Mathematical Tables*, 28th ed.; CRC Press: Boca Raton, FL, 1987.
(46) Gottschalk, M.; Venu, K.; Halle, B. *Biophys. J.* **2003**, *84*, 3941−3958.

$$\frac{F_{\text{prim}}}{kT} \approx \frac{U_{\text{ads}}}{kT} + \frac{V_{\text{protein}}}{\Sigma^{3/2}} - \zeta \frac{A_{\text{protein}}}{\Sigma^{1/2}\xi_{\text{ad}}} \approx \frac{U_{\text{ads}}}{kT} + \left(\frac{\Sigma_{\text{ads}}}{\Sigma}\right)^{1/2}\left(\frac{\Sigma_{\text{co}}^{\text{tern}}}{\Sigma} - \zeta\right) \quad (22)$$

where $\zeta < 1$ is a numerical constant allowing for the effects of the proximity of the impenetrable surface on the PEG adsorption onto the protein. For example, a protein at the surface is likely to experience fewer contacts with the PEG chains because it is shielded by the surface. Note that ζ may be affected by other factors such as surface roughness and may well vary from one protein to another. In addition, adsorption at the surface may be associated with structural changes. These will not affect V_{protein} but may modify A_{protein} at the surface. Overall, the importance of the third term, the PEG−protein attraction term, depends on the value of ζ as well as ϵ. The uncertainty in ϵ is especially important. If one is to assume $\epsilon = 0.01$ instead of $\epsilon = 0.05$, then the adsorption free-energy term will be strongly reduced, and eq 3 will provide a valid description of the system. Because typically both ζ and ϵ are unknown, the choice between eqs 3 and 22 is currently dictated by the experimental data.

Within our model, when $U_{\text{ads}} < 0$ and $\epsilon < 0$ the adsorbed amount $\Gamma \approx N_{\text{tot}}$ is given by (eq 1), $N_{\text{tot}} = N_{\text{prim}} + N_{\text{tern}} \approx (K_{\text{prim}} + K_{\text{tern}})c_{\text{p}}$, where K_{tern} is specified by eq 16 and K_{prim} for a fully inserted protein is

$$K_{\text{prim}} \approx N_{\text{prim}}^{\max} \exp\left[\frac{|U_{\text{ads}}|}{kT} - \left(\frac{\Sigma_{\text{ads}}}{\Sigma}\right)^{1/2}\left(\frac{\Sigma_{\text{co}}^{\text{tern}}}{\Sigma} - \zeta\right)\right] \quad (23)$$

K_{prim} exhibits a maximum at $\Sigma_{\max} = 2\Sigma_{\text{co}}^{\text{tern}}/\zeta$ due to the competition between PEG−protein attractions and the osmotic penalty. The relative importance of K_{prim} and K_{tern} varies with the brush thickness $H \sim N$ and thus with the PEG degree of polymerization N. $N_{\text{prim}}^{\max}$ is independent of N but varies with σ_{ads}, the area occupied by an adsorbed protein. Its upper bound, in the limit of close packing, is $N_{\text{prim}}^{\max} = 1/\sigma_{\text{ads}}$. In contrast, $K_{\text{tern}} \sim N$. The saturation value for N_{tern} scales roughly as H/d_{protein}, where d_{protein} is the relevant dimension of the protein. For approximately spherical proteins, d_{protein} is larger but comparable to their radius, R. For proteins having the shape of prolate ellipsoids, d_{protein} is determined by their minor semiaxis. The ternary adsorption contribution to Γ is thus dominant when $H/d_{\text{protein}} \gg 1$. However, when $H/d_{\text{protein}} \lesssim 1$ pure ternary adsorption is impossible, and Γ is due to the primary adsorption of partially inserted proteins as modified by the PEGp-protein attraction specified by the ϵ value for the protein in question.

VII. Marginal Solvent versus Good Solvent

Our analysis thus far considered PEG to be a flexible chain immersed in a good solvent. The evidence that water is a good solvent for PEG mostly concerns the high N range.[23−26] Recent analysis of π versus ϕ data suggests, however, that solutions of short PEG chains, $N \lesssim 50$, deviate from the $\pi \approx kT/\xi^3 \approx \phi^{9/4}$ behavior expected in good solvent[27] and exhibit mean-field (MF) $\pi \approx \phi^2$ scaling.[28] In turn, such MF behavior will modify both F_{osm} and F_{ads} as obtained earlier assuming good solvent conditions. Whereas the modifications will not affect the qualitative features of our analysis, they merit discussion for the following reasons: First, a number of physical chemistry experiments and the majority of practical applications involve PEG chains with $N \lesssim 50$. Second, as we shall discuss, MF behavior may affect brushes of longer chains at high grafting densities. Finally, it is a factor to bear in mind when considering the quantitative comparison between theory and experiment.

In the following text, we base our discussion on the state diagram of semiflexible "simple polymers" that undergo phase separation upon cooling to below their Θ temperature[47,48] and utilize the reduced temperature $\tau = 1 - \Theta/T$. However, we should first note certain reservations concerning the applicability of this analysis to short PEG chains. Two issues are involved. First, PEG undergoes phase separation upon heating, a feature typically rationalized by introducing two-state models.[49−54] In contrast, the theory of simple polymers, where the monomers exist in a single state, allows for phase separation only upon cooling. Second, this approach ignores the role of chain ends whose importance grow as N decreases. With these caveats in mind, we first summarize the relevant features of the state diagram of semiflexible chains where MF behavior is traceable to the chain rigidity as characterized by its Kuhn length l. In particular, regions of MF behavior occur when Kuhn length l comprises $p > 1$ monomers. This analysis is formulated in terms of $\tau = 1 - \Theta/T$ and is thus strictly applicable only to polymers undergoing phase separation upon cooling. For simplicity, we will utilize τ in our discussion of PEG in spite of its different phase behavior. However, when applied to PEG, τ denotes an unspecified dimensionless function of T rather than $\tau = 1 - \Theta/T$. Note that whereas there is no consensus over the values of l, p, and C_∞ of PEG, the reported values suggest $1 < p \leq 3$.[24,55]

The introduction of $p > 1$ affects three aspect of the chain behavior as discussed within a Flory-type theory.[47] First, the elastic free energy, $F_{\text{el}}/kT \approx (R/R_{\text{o}})^2$ is weakened because the radius of a random walk of Kuhn segments is $R_0/a \approx (N/p)^{1/2}p = (Np)^{1/2} > N^{1/2}$. Second, two mutually canceling changes occur in the interaction free energy $F_{\text{int}}/kT \approx \upsilon c^2 R^3$. Viewing the two interacting monomers as cylinders leads, following Onsager theory, to a second virial coefficient $\upsilon \approx l^2 a\tau = p^2 a^3 \tau$ instead of $\upsilon \approx a^3\tau$ for a flexible chain. At the same time, the monomer concentration $c = N/R^3$ is replaced by the concentration of Kuhn segments N/pR^3. The corresponding Flory radius, as specified by the minimum of $F_{\text{chain}}(R) = F_{\text{el}} + F_{\text{int}}$ when $F_{\text{el}} \approx F_{\text{int}}$, is thus increased to $R_{\text{F}}/a \approx (p\tau)^{1/5}N^{3/5}$. However, the chain retains its random walk statistics, with $R \approx R_0$, as long as F_{int} is sufficiently small and its effect on the chain configurations is weak. The boundary between this MF marginal solvent domain and the self-avoidance good solvent regime characterized by R_{F} is determined by the condition $F_{\text{int}}(R_{\text{F}}) \approx kT$ or alternatively $F_{\text{int}}(R_0) \approx kT$. Both yield a crossover at $N_{\text{r}} = p^3/\tau^2$ corresponding to $R_0 \approx R_{\text{F}}$. In particular, $F_{\text{int}}(R_0)/kT \approx (N/N_{\text{r}})^{1/2}$ whereas $F_{\text{int}}(R_{\text{F}})/kT \approx (N/N_{\text{r}})^{1/5}$ and $F_{\text{int}}(R_0) < F_{\text{int}}(R_{\text{F}})$ for $N \leq N_{\text{r}}$, thus leading to a random walk configuration in this range. Self-avoidance leading to R_{F} occurs at $N > N_{\text{r}}$ when $F_{\text{int}}(R_0) > F_{\text{int}}(R_{\text{F}})$. The Flory radius for $N = N_{\text{r}}$ thus defines the smallest blob size exhibiting self-avoidance, $\xi_{\text{r}}/a \approx p^2/\tau$. Consequently, the boundary between MF and good solvent behavior occurs at $\phi_{\text{r}} \approx N_{\text{r}}a^3/\xi_{\text{r}}^3 \approx \tau/p^3$, and MF behavior is expected at $\phi > \phi_{\text{r}}$. In a brush, the crossover occurs at $\Sigma_{\text{r}} \approx \xi_{\text{r}}^2 \approx p^4/\tau^2$. In the good solvent regime, $\pi a^3/kT \approx (\tau p)^{3/4}\,\phi^{9/4}$ corresponding to kT per blob or $\pi \approx kT/\xi^3$.

(47) Schaefer, D. W.; Joanny, J. F.; Pincus, P. *Macromolecules* **1980**, *13*, 1280−1289.
(48) Birshtein, T. M.; Zhulina, E. B. *Polymer* **1984**, *25*, 1453−1461.
(49) Goldstein, R. *J. Chem. Phys.* **1984**, *80*, 5340−5341.
(50) Karlstrom, G. *J. Phys. Chem.* **1985**, *89*, 4962−4964.
(51) Matsuyama, A.; Tanaka, F. *Phys. Rev. Lett.* **1990**, *65*, 341−344.
(52) Dormidontova, E. *Macromolecules* **2002**, *35*, 987−1001.
(53) Bekiranov, S.; Bruinsma, R.; Pincus, P. *Europhys. Lett.* **1993**, *24*, 183−188.
(54) Bekiranov, S.; Bruinsma, R.; Pincus, P. *Phys. Rev. E* **1997**, *55*, 577−585.
(55) Rubinstein, M.; Colby, R. H. *Polymer Physics*; Oxford University Press: Oxford, U.K., 2003.

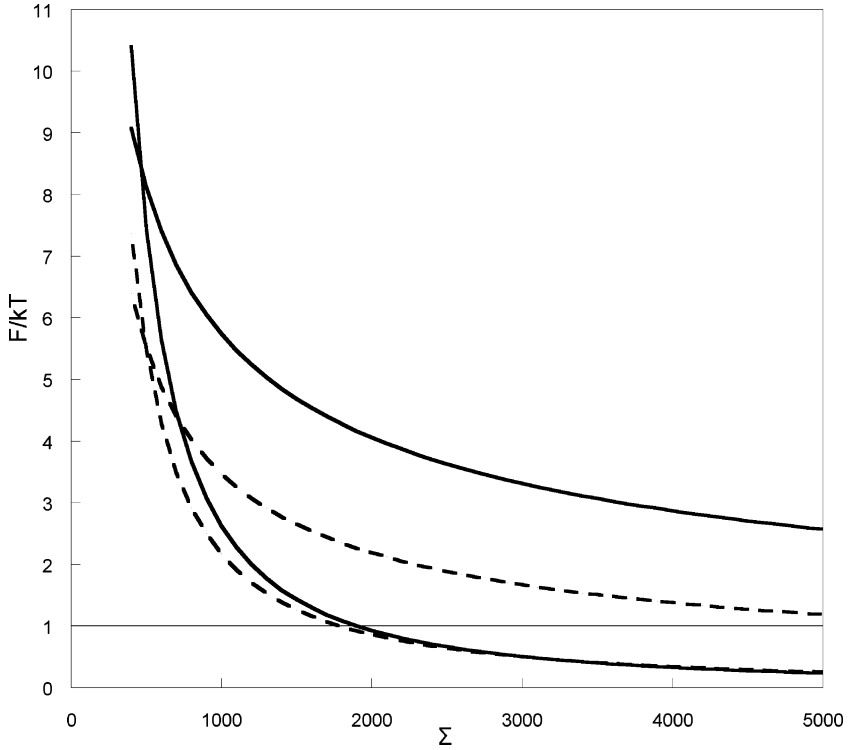

Figure 5. Plots of F_{osm}/kT (eq 2), F_{osm}^{MF}/kT (eq 25), F_{ads}/kT (eq 12), and F_{ads}^{MF}/kT (eq 26) vs Σ for $p = 2$, $\tau = 0.25$, $a = 3.5$ Å, and $V_{protein} = 8.3 \times 10^4$ Å^3 corresponding to triangular BSA. The lower two curves correspond to F_{ads}/kT and F_{ads}^{MF}/kT, and the upper two correspond to F_{osm}/kT and F_{osm}^{MF}/kT. The MF and good solvent results are depicted respectively by (---) and (−). The intersection between F_{ads}/kT (F_{ads}^{MF}/kT) and $F = 1$ specify Σ_{ads} (Σ_{ads}^{MF}) whereas the intersection of F_{osm}/kT (F_{osm}^{MF}/kT) and F_{ads}/kT (F_{ads}^{MF}/kT) determine Σ_{co}^{tern} (Σ_{co}^{ternMF}).

In the MF marginal solvent domain, where unscreened binary monomer−monomer interactions dominate, $\pi_{MF}a^3/kT \approx \tau\phi^2$.[47,48]

To apply this picture to our system, it is first necessary to specify τ and p of aqueous PEG solutions at ambient temperature. An analysis of π of PEG solutions[27] showed that the good solvent behavior can be described by $\pi a^3/kT \approx \alpha\phi^{9/4}$ with $\alpha = 0.8$. Comparison to $\pi a^3/kT \approx (\tau p)^{3/4}\phi^{9/4}$ thus leads to $\tau \approx \alpha^{4/3}/p$ and $N_r \approx p^5/\alpha^{8/3}$. For $p = 3$, this leads to $N_r \approx 430$, but for $p = 2$, it results in $N_r \approx 58$. Because MF $\pi \approx \phi^2$ scaling was found for $N \lesssim 50$, this argument suggests that $p = 2$ and $\tau \approx 0.25$, leading to $\xi_r \approx 56$ Å, $\phi_r \approx 3.12 \times 10^{-2}$, and $\Sigma_r \approx 3140$ Å^2.

The general features of our earlier discussion concerning good solvent behavior apply also to the MF regime. However, three modifications are necessary. One concerns the boundary of the weak adsorption regime. For a Gaussian chain of Kuhn segments, the adsorption blob size is $\xi_{ad}^{MF} \approx pa/\epsilon$.[55] Weak adsorption occurs when ξ_{ad}^{MF} is larger than the marginal solvent screening length $\xi^{MF}/a \approx p^{1/2}\tau^{-1/2}\phi^{-1/2} \approx p^{2/3}\tau^{-1/3}(\Sigma/a^2)^{1/3}$.[47,48] The second concerns the osmotic penalty. Because $\pi_{MF}a^3/kT \approx \tau\phi^2$ replaces $\pi \approx kT/\xi^3$ but $H/a \approx N(\tau p a^2/\Sigma)^{1/3}$ is unaffected,[48] the osmotic penalty becomes

$$\frac{F_{osm}^{MF}}{kT} \approx \frac{\pi_{MF}V_{protein}}{kT} \approx \frac{\tau V_{protein}}{a^3}\left(\frac{Na^3}{H\Sigma}\right)^2 \approx \frac{\tau^{1/3}V_{protein}}{a^3p^{2/3}}\left(\frac{a^2}{\Sigma}\right)^{4/3} \quad (24)$$

Finally, in the MF regime it is reasonable to estimate the number of monomer−protein contacts as $cA_{protein}a$, where c is the PEG monomer concentration in the brush. Accordingly,

$$\frac{F_{ads}^{MF}}{kT} \approx -\frac{A_{protein}\epsilon}{a^2(\tau p)^{1/3}}\left(\frac{a^2}{\Sigma}\right)^{2/3} \quad (25)$$

The scaling behavior in the two regimes is, as expected, somewhat different: $(a^2/\Sigma)^{4/3}$ versus $(a^2/\Sigma)^{3/2}$ for F_{osm} and $(a^2/\Sigma)^{2/3}$ versus $(a^2/\Sigma)^{1/2}$ for F_{ads}. This also affects the boundaries of the adsorption regimes. For example, the onset and end of the ternary adsorption range in the MF regime are

$$\frac{\Sigma_{ads}^{MF}}{a^2} \approx \frac{(\epsilon A_{protein})^{3/2}}{a^3(\tau p)^{1/2}}\ ;\ \frac{\Sigma_{co}^{ternMF}}{a^2} \approx \frac{\tau}{p^{1/2}}\left(\frac{V_{protein}}{a\epsilon A_{protein}}\right)^{3/2} \quad (26)$$

Both $F_{osm}/F_{osm}^{MF} \approx p^{2/3}\tau^{-1/3}(a^2/\Sigma)^{1/6}$ and $F_{ads}/F_{ads}^{MF} \approx (\tau p)^{1/3}$ $(\Sigma/a^2)^{1/6}$ vary slowly with Σ. When $\Sigma > \Sigma_r$, the MF free energies are lower though the numerical values are similar for $\Sigma > 600$ Å^2. The behavior of F_{osm}, F_{osm}^{MF}, F_{ads}, and F_{ads}^{MF} for $p = 2$ and $\tau = 0.25$ is depicted in Figure 5 for the case of fully inserted triangular BSA and the experimentally relevant Σ range.

The relative simplicity of the expressions for F_{osm} and F_{ads} in the good solvent regime is traceable to the Alexander picture of a brush comprising nonoverlapping close-packed blobs of size $\xi \approx \Sigma^{1/2}$. In the MF range, $\pi \approx kT/\xi^3$ does not apply, and the blobs overlap,[48] thus giving rise to more cumbersome expressions exhibiting τ and p dependencies. Because of the simplicity of the blob picture and the uncertainties concerning p and τ, we will base our discussion of the experimental results (section VIII) on the good solvent blob expressions.

VIII. Comparison to Experiment

The main outcome of the theory presented above are protein adsorption isotherms of surfaces coated by PEG brushes and immersed in a protein solution. In common with preceding theoretical approaches, it considers protein adsorption as a reversible process and focuses on the equilibrium situation.[6,7,9,10] Our theory is strictly applicable to stationary and path-independent

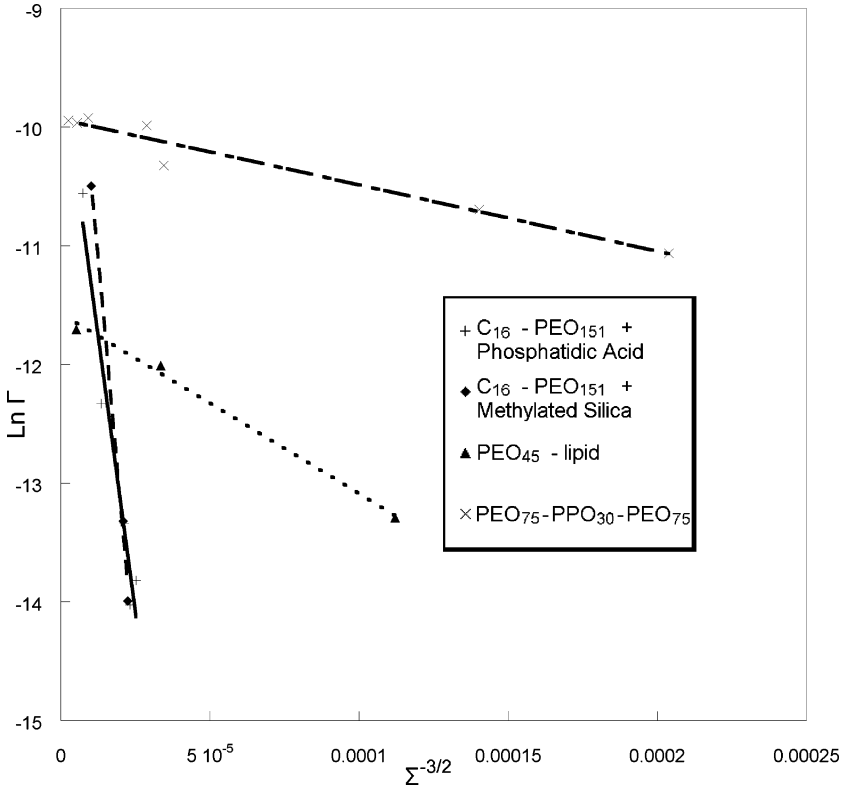

Figure 6. Plots of ln Γ vs $\Sigma^{-3/2}$ utilizing the fibrinogen Γ(Σ) data as reported by Malmsten and van Alstine,[13] Efremova et al.,[11] and McPherson et al.[12] ($C_{16}-PEO_{151}$ corresponds to ref 13, $PEO_{45}-$lipids corresponds to ref 11, and $PEO_{75}-PPO_{30}-PEO_{75}$ corresponds to ref 12).

equilibrium states. It is nevertheless expected to capture the essential features of the adsorption behavior when the deviation from equilibrium is small. As discussed earlier, it allows us to rationalize the qualitative trends in the dependence of Γ on Σ and *N*. As we shall see, the adsorption isotherms also allow us to fit experimental data, and the parameters thus obtained are consistent with the theory. However, before we discuss these fits it is important to list a number of difficulties confronting quantitative comparison between theory and experiment. These fall into three categories. One concerns equilibrium and equilibration. Within this category, the first difficulty concerns the time scales for attaining true Γ plateau values. The kinetics of adsorption are expected to vary with Σ, *N*, c_p, and the mixing or flow conditions used. The identification of a plateau regime may well vary with the observation time and the sensitivity of the measurement method. The uncertainties involved are illustrated by the following observations: in the experiment of Malmsten and Van Alstine,[13] most proteins adsorb within 5 min, but the subsequent slower adsorption contributed an extra 25% of Γ within the following 75 min. Bosker et al.[14] reported that a plateau in Γ was typically attained within the observation time of 90 min. They note, however, that the adsorption at low Σ values is very slow and longer equilibration is necessary to attain "true plateau" values. In contrast, Norde and Gage monitored Γ for 30 min and reported the attainment of plateau values after 3−5 min.[15] Second, there is currently little information on the kinetics of protein desorption out of surfaces coated with PEG brushes. This is of practical interest when the measurement of Γ involves a rinsing step. It is also of fundamental importance for establishing the role of hysteresis and thus for determining the applicability of equilibrium thermodynamics models assuming reversible protein adsorption. Additionally, it is important to note that ternary and primary adsorption may well differ in their kinetics. The second category of difficulties concerns the uncertainties in the parameters utilized in the model. These fall into two groups. The proteins and their interactions are characterized by U_{ads}, $V_{protein}$, $A_{protein}$, and ϵ. As we discussed earlier, these parameters are available only for a limited set of proteins, and the reported values are occasionally subject to debate and may require revision. The second set of parameters, Σ and *N*, characterizes the brush. Here it is important to note that the reported Σ values are averages and that nonuniformities in coverage may lead to significant contributions to Γ. The final category of difficulties is associated with the use of the Alexander model, the approximations involved, and the neglect of numerical factors of order unity. It also includes the uncertainties concerning the MF domain of PEG and its brushes.

It is of interest to note that physical chemistry experiments concerning the interactions between PEG brushes and proteins fall, in effect, into two groups. In one, the brushes are produced from PEG−lipids,[11,13] and in the second, they are composed of block copolymers.[7,14,15] In practice, the two groups differ in the *N* range explored. The longer PEG lipids that are commercially available comprise PEG blocks of $N = 45$ and 113.[56] The longest PEG lipid conjugate reported comprised $N = 270$.[57] In contrast, PS−PEO block copolymers allowed us to probe a significantly larger range of $48 \leq N \leq 770$. The *N* range determines the accessible brush heights as well as the maximal attainable Σ.

With these observations in mind, we present below four fits utilizing the good solvent versions of the adsorption isotherms. The first (Figure 6) concerns fibrinogen Γ(Σ) data as reported by Malmsten and van Alstine,[13] Efremova et al.,[11] and McPherson et al.[12] All plots of ln Γ versus $\Sigma^{-3/2}$, as suggested by eq 5, exhibit linear behavior. However, the data of Malmsten and van Alstine yields $V_{protein} \approx 2 \times 10^5$ and 2.7×10^5 Å^3 comparable to the anhydrous $V_{protein}$ of fibrinogen. In contrast, the data of Efremova et al. and McPherson et al. yield much smaller values of $V_{protein}$.

(56) www.avantilipids.com/SytheticFuncionalizedPegLipids.asp.
(57) Bedu-Addo, F. K.; Tang P.; Xu Y.; Huang L. *Pharm. Res.* **1996**, *13*, 718−724.

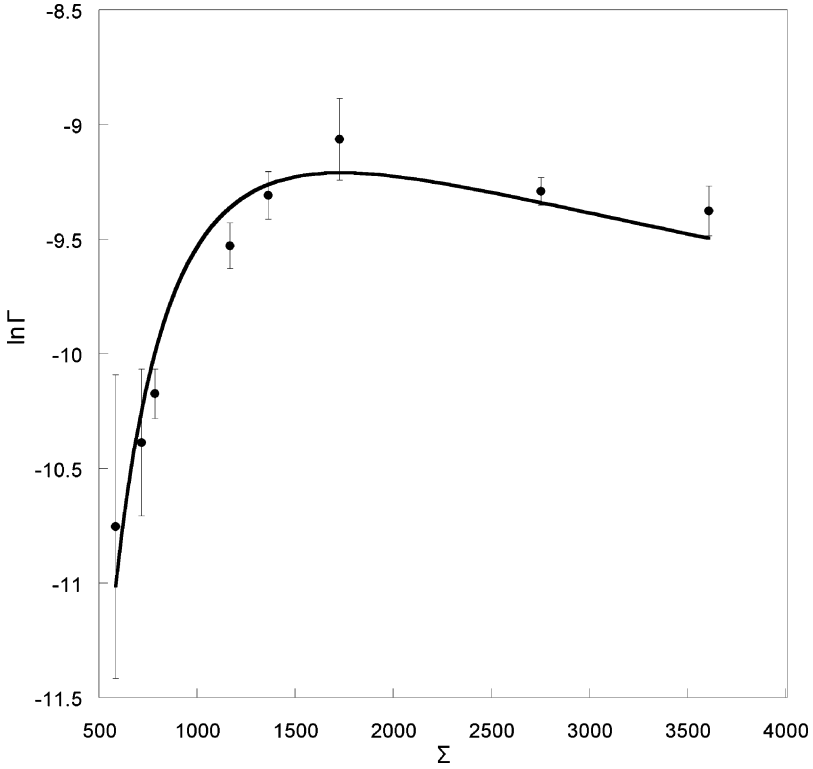

Figure 7. Fit of the ln Γ(Σ) of BSA adsorption onto a PEG brush with $N = 770$ as reported by Bosker et al.[14] using eq 16 for pure ternary adsorption.

The second fit of ln Γ (Figure 7) utilizes the data of Bosker et al.[14] concerning the adsorption of BSA onto PEG brushes with $N = 770$. The data is fitted to eq 16, allowing for pure ternary adsorption that dominates Γ for high N. It yields $V_{protein} = 5.85 \times 10^4$ Å^3 and $A_{protein} = 3.2 \times 10^4$ Å^2, which are comparable to the BSA model values. Notice further that eq 18 for BSA and $\epsilon = 0.05$ yields $\Sigma_{max} \approx 1300$ Å^2, which is close to the experimentally observed value of $\Sigma_{max} \approx 1700$ Å^2. Whereas the predicted Σ_{max} vary with the assumed geometry, both models yield similar values. Note that the measured Γ values incorporate contributions due to primary adsorption at the surface. Bosker et al. tried to eliminate this contribution by utilizing bimodal brushes formed by a mixture of $N = 770$ and 48 where the dense $N = 48$ inner brush aimed to suppress primary adsorption.[14] However, the analysis of Γ(Σ) of the binary PEG brush requires a more elaborate model.

The Γ(Σ) data of Bosker et al.[14] concerning the adsorption of BSA onto PEG brushes of $N = 48$ can be fitted using eq 5. The linear fit obtained for the ln Γ versus $\Sigma^{-3/2}$ plots leads, however, to $V_{protein} \approx 5.2 \times 10^3$ Å^3, a value that is much smaller than $V_{protein}$ suggested by the BSA models. This discrepancy arises because eq 5 does not allow for two relevant ingredients. One is the possibility of partial insertion. The second is the effect of BSA−PEG attraction at the surface. The Σ range explored, 170 Å$^2 \le \Sigma \le 900$ Å^2, corresponds to $H/a \approx N(a^2/\Sigma)^{1/3}$ with 11.5 Å $\lesssim H \lesssim$ 20 Å. This suggests that partial insertion plays a role irrespective of the BSA model invoked, yet fitting with the partial insertion model for BSA undergoing pure primary adsorption (eq 7) does not result in significant improvement in the value of $V_{protein} \approx 5.2 \times 10^3$ Å^3. We next fitted the data using eq 23, allowing for primary adsorption and PEG−protein attraction and where $V_{protein}$ was replaced by $V_{in} \approx 3.0 \times 10^5$ Å^3 as suggested by the triangular model for $H \approx 14$ Å. The prefactor of the $\Sigma^{-1/2}$ term was found to be 3.2×10^2 Å as compared to $A_{protein}/\xi_{ad} \approx 1.8 \times 10^2$ Å predicted by the theory for the triangular model and $\epsilon = 0.05$ (Figure 8). The fit was obtained upon elimination of one data point corresponding to $\Sigma \approx 850$ Å^2 where the experimental error, according to Bosker et al., was especially high.

The last plot (Figure 9) concerns the results of Norde and Gage,[15] who measured Γ of BSA as a function of N for $90 \le N \le 700$ at constant $\Sigma \approx 1 \times 10^3$ Å and c_p. Importantly, Γ displays a minimum around $N = 250$. The decrease in Γ for $90 \le N < 250$ may be rationalized within the partial insertion picture for the triangular wedge model of BSA, assuming that the protein adsorbs with its narrow edge parallel to the surface. The height of a sideways-adsorbed BSA is $h \approx 70$ Å, and the validity of this interpretation depends crucially on the brush thickness, H. The athermal estimate $H/a \approx N(a^2/\Sigma)^{1/3}$ leads to $H \approx 73$ Å $\gtrsim h$ for the shorter chains with $N = 90$, thus ruling out this scenario. Using $H/a \approx (p\tau)^{1/3}N(a^2/\Sigma)^{1/3}$ with $p = 2$, $\tau = 0.25$, and $N = 90$ yields $H \approx 58$ Å, supporting the partial insertion interpretation. The H values calculated by Norde and Gage for $N = 90$ and 148 also support this picture. A quantitative analysis of the $0 \le N < 250$ range in terms of the partial insertion picture is, however, difficult because the model does not apply to the bare surface and because the $N = 148$ brush may well correspond to full insertion. For $250 \le N \le 700$, we expect ternary adsorption to dominate Γ. For $\Sigma = \text{const}'$, eq 16 leads to $\ln \Gamma \approx \ln N + \text{const}'$, thus suggesting the plot of ln Γ versus ln N. The resulting plot (Figure 9) is linear, but the slope is roughly 2 whereas the theory predicts a slope of unity. This difference may reflect a N dependence of Σ.

A final comment concerns general aspects of the experimental design of surfaces that are resistant to protein adsorption using PEG brushes. The current practice favors PEG brushes with $N \lesssim 100$. Our considerations suggest a qualitative rationalization of this common choice. The performance of protein-repellent brushes is determined primarily by the grafting density or Σ. This determines the osmotic penalty $F_{osm} \approx kTV_{protein}/\Sigma^{3/2}$ that opposes both primary and ternary adsorption, thus advocating high grafting densities or small Σ. The role of N is twofold. On the positive side, secondary adsorption at the outer edge of the

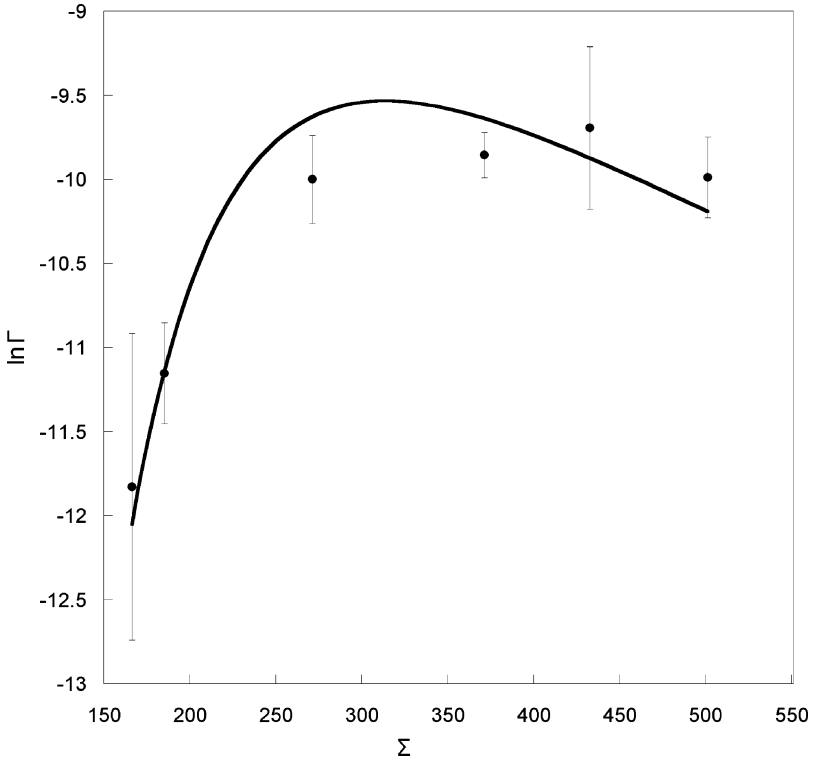

Figure 8. Fit of the ln Γ(Σ) of BSA adsorption onto a PEG brush with $N = 48$ as reported by Bosker et al.[14] using eq 23, which allows for primary adsorption and PEG−protein attraction. $V_{protein}$ was replaced by $V_{in} \approx 3.0 \times 10^5$ Å^3 as suggested by the triangular model for $H \approx 14$ Å.

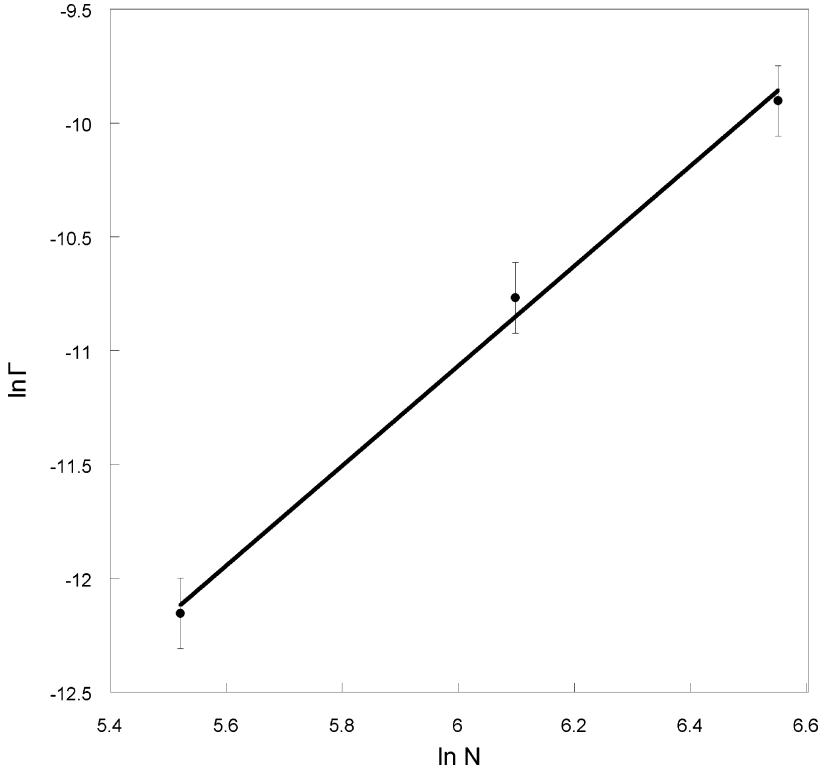

Figure 9. Plot of ln Γ vs ln N for BSA adsorption onto a PEG brush with $250 \leq N \leq 770$ and constant $\Sigma = 1000$ Å^2 as reported by Norde and Gage.[15]

brush is weakened as $H \approx N(a^2/\Sigma)^{2/3}a$ increases with N because of the lowering of the van der Waals attraction experienced by the protein.[6] As we discussed, it also avoids lower F_{osm} because of partial insertion. On the negative side, larger N favor undesirable ternary adsorption because $K_{tern} \sim N$. This last effect can be avoided if the grafting density is high enough, $\Sigma < \Sigma_{co}^{tern}$. However, this remedy is not always possible because of the adverse effect of N on the attainable grafting density.[6] This arises because the free energy per brush chain scales as $N(a^2/\Sigma)^{5/6}$. High grafting densities are thus difficult to attain for high N because of slower kinetics or because the anchoring free energies are too low. Finally, at present there is direct experimental

evidence for the occurrence of both primary and ternary adsorption but no similar indications of secondary adsorption. Altogether, these considerations, together with practical difficulties in synthesizing longer chains, favor the use of high grafting densities and shorter chains.

IX. Discussion

The design of PEG brushes that resist protein adsorption involves, in the simplest case, two parameters, Σ and N. These control both primary adsorption at the surface and ternary adsorption within the brush. Earlier theories concerning these systems considered fully inserted proteins while focusing on primary adsorption in the absence of ternary one or visa versa. Furthermore, the discussion of ternary adsorption invoked the assumption that PEG strongly adsorbs onto proteins, in contradiction to experimental observation in the bulk. In contrast, our analysis allows for concurrent primary and ternary adsorption and partial insertion of large proteins into "shallow" brushes while utilizing the weak adsorption limit to describe PEG−protein interactions. This accounts for three leading qualitative trends: (i) the monotonic decrease of Γ with Σ for low N where ternary adsorption is negligible; (ii) the maximum in $\Gamma(\Sigma)$ for large N when ternary adsorption is dominant; and (iii) the minimum in $\Gamma(N)$ for constant Σ as a result of incomplete insertion of large proteins at low N. Furthermore, the simple explicit expressions for the adsorption isotherms allow us to fit experimental data and yield parameters in semiquantitative agreement with the theory.

Our analysis has the merit of producing simple closed-form expressions and a transparent physical picture. These advantages were gained at the price of simplifying assumptions briefly introduced earlier. Here we again list the key assumptions and their consequences. Theories rationalizing the phase behavior of PEG incorporate two-state models assuming that each PEG monomer undergoes dynamic equilibration between a hydrophilic and a hydrophobic state.[49−54] The precise identification of the interconverting states varies between the different models, but all view PEG as an annealed heteropolymer. In contrast, the theoretical approach presented above and the preceding efforts in this area view PEG as a homopolymer comprising a single type of monomer. Another important common approximation is the assumption that a protein can be modeled as having a uniform surface, thus neglecting the existence of hydrophobic and hydrophilic domains. Imposing these two assumptions allows us to describe PEG−protein interactions in terms of a single parameter ϵ. Other, more evident assumptions were invoked. First, our analysis of the insertion mode ignores the effects of the protein's entry on the brush structure. Second, the Alexander model assumes a steplike concentration profile with a constant ξ. A more refined SCF theory yields a parabolic concentration profile with a height-dependent ξ, thus leading to a height dependent F_{ads} and F_{osm}. Also, the precise boundaries of the MF regime of PEG and the associated parameters remain to be determined. Finally, our discussion did not allow for the role of electrostatic interactions, thus implying proteins at their isoelectric points. However, it is important to note that electrostatic interactions among overly neutral proteins may also arise because of higher electric moments of the proteins or the capacity of PEG to bind cations.[58]

It is useful to highlight the main differences between our discussion and an earlier model of pure ternary adsorption proposed by Currie et al.[7] First, Currie et al. considered the strong adsorption limit when the PEG chains bind individual proteins and form string of pearls configurations. As noted by the authors, this picture is not consistent with their light scattering measurements that show no aggregation between PEG and BSA in the bulk. In line with the string of pearls model, their analysis invokes an ideal mixing entropy associated with the placement of proteins along a single chain. In contrast, within our picture an adsorbed protein does not "belong" to a single chain, and the entropy of the proteins is $S \simeq kN_{tern} \ln(eH/N_{tern})$. Second, in contrast to our treatment, the number of monomers in contact with a given protein in the model of Currie et al. is an adjustable parameter that does not depend on Σ, ϵ, or $A_{protein}$. Finally, the strong adsorption assumption suggests that protein may undergo ternary adsorption in the mushroom regime whereas within our model ternary adsorption can occur only in the brush range.

To conclude, it is of interest to comment on a key experimental issue. Thus far, the evidence distinguishing primary and ternary protein adsorption is indirect. It is based on the variation of the amount of adsorbed protein Γ with respect to Σ and N. Direct experimental discrimination between the two adsorption mechanisms requires characterization of the protein concentration profile within the brush. A technique that may permit such characterization is neutron reflectivity when implemented with deuterated proteins.

X. Appendix I: $\Phi = {}^1/_2$ versus $\Phi \approx {}^3/_5$

Our discussion follows the blob analysis of Bouchaud and Daoud,[33] thus utlizing $\Phi \approx {}^3/_5$ as motivated by $\Phi \approx 0.58$ obtained by Eisenriegler, Kremer, and Binder[60] from Monte Carlo (MC) simulation results. Later, an MC study by Meirovich and Livne[61] led to $\Phi \approx 0.530$. The results of more recent MC studies[62,63] are consistent with $\Phi = {}^1/_2$. The use of $\Phi = {}^1/_2$ instead of $\Phi \approx {}^3/_5$ does not affect the qualitative aspects of the analysis but resuls in somewhat different expressions as summarized below.

Because an adsorption blob is defined via $g_{ad}^{\Phi}\epsilon \approx 1$ and $\xi_{ad} \approx g_{ad}^{3/5}a$, the use of $\Phi = {}^1/_2$ leads to

$$g_{ad} \approx \epsilon^{-2} \text{ and } \xi_{ad} \approx a/\epsilon^{6/5} \tag{27}$$

In turn, this modifies $F_{ads}/kT \approx -(A_{protein}/\xi^2)g^{\Phi}\epsilon$, leading to

$$\frac{F_{ads}}{kT} \approx -\frac{A_{protein}}{\Sigma^{7/12}\xi_{ad}^{5/6}} \approx -\left(\frac{\Sigma_{ads}}{\Sigma}\right)^{7/12} \tag{28}$$

and

$$\frac{F_{tern}}{kT} \approx \left(\frac{\Sigma_{ads}}{\Sigma}\right)^{7/12}\left[\left(\frac{\Sigma_{co}^{tern}}{\Sigma}\right)^{11/12} - 1\right] \tag{29}$$

where

$$\Sigma_{ads} \approx \frac{A_{protein}^{12/7}}{\xi_{ad}^{10/7}} \text{ and } \Sigma_{co}^{tern} \approx \left(\frac{V_{protein}}{A_{protein}}\right)^{12/11}\xi_{ad}^{10/11} \tag{30}$$

XI. Appendix II: Scaling Regimes of Pure Ternary Adsorption

Within a puristic scaling analysis, ignoring numerical factors due to geometry, it is possible to distinguish between three types

(58) (a) Cross, J. In *Nonionic Surfactants: Chemical Analysis*; Cross, J, Ed.; Marcel Dekker: New York, 1987. (b) Zhivkova, I. V.; Zhivkov, A. M.; Stoychev, D. S. *Eur. Polym. J.* **1998**, *34*, 531−538.
(59) Moore, W. J. *Physical Chemistry*; Longman: London, 1972.
(60) Eisenriegler, E.; Kremer, K.; Binder, K. *J. Chem. Phys.* **1982**, *77*, 6296.
(61) Meirovich, H.; Livne, S. *J. Chem. Phys.* **1988**, *88*, 4507.
(62) Heger, R.; Grassberger, P. *J. Phys. A: Math. Gen.* **1994**, *27*, 4069−4081.
(63) Metzger, S.; Muller, M.; Binder, K.; Baschnagel, J. *J. Chem. Phys.* **2002**, *118*, 8489.

Table 3

object	$V_{protein}$	$A_{protein}$	$V_{protein}/A_{protein}\xi$
spheres	R^3	R^2	R/ξ
cylinders ($L \gg R$)	R^2L	RL	R/ξ
disks ($R \gg H$)	R^2H	R^2	H/ξ

of "proteins", spheres, long cylinders corresponding to extended prolate ellipsoids, and thin disks corresponding to narrow oblate ellipsoids. The spheres are characterized by their radius R. The radius R of the cylinders is much smaller than their length L whereas the radius of the disks R is much larger than their width H. The weak adsorption regime is defined by the condition $F_{osm}/F_{ads} < 1$ and $\xi < \xi_{ad}$. Accordingly, $F_{osm}/F_{ads} \approx (V_{protein}/A_{protein}\xi)$-$(\xi_{ad}/\xi) < 1$, thus leading to $(V_{protein}/A_{protein}\xi) < \xi/\xi_{ad} < 1$. The scaling behavior of the three objects is summarized in Table 3.

For spheres, the weak scaling regime condition implies that $R < \xi$ and thus $V_{protein} < \xi^3$, where the applicability of $F_{osm}/kT \approx V_{protein}/\xi^3$ is questionable. The situation is more favorable for cylinders and disks where the weak adsorption regime requires $R < \xi$ and $H < \xi$. In contrast to the spheres, in these last two cases $V_{protein} > \xi^3$ is possible though one of the dimensions is smaller than ξ. These difficulties on the scaling level do not necessarily rule out the existence of the weak adsorption regime. Rather, they indicate that the weak adsorption range is determined by numerical factors. The experimental observations of protein adsorption onto PEG brushes and of the absence of PEG−protein complexation in solution suggest that weak adsorption should indeed be considered.

XII. Appendix III: Reversible versus Irreversible Primary Adsorption

The equilibrium isotherm of primary adsorption of a fully immersed protein onto a surface coated with a PEG brush gives rise to a characteristic dependence of Γ on Σ. For pure primary adsorption $\epsilon = 0$ from a good solvent, this leads to $\ln N_{prim} \approx \text{const}' - V_{protein}/\Sigma^{3/2}$. As discussed in section VIII, this form well describes certain measurements. However, because the attainment of thermodynamic equilibrium is yet to be established, it is of interest to note that such $\Gamma(\Sigma)$ may reflect a kinetic effect. In particular, it may be due to irreversible adsorption if the adsorption rate constant, k_{ad}, reflects an activation free energy due to the osmotic penalty, $\pi V_{protein}$, associated with entry into the brush.[6,9] To illustrate this point, we consider the simplest case when protein transport towards the surface does not affect the adsorption rate. In this situation, when there is no desorption, the adsorption rate equation is

$$\frac{d\theta}{dt} = k_{ad}(1 - \theta)c_p \tag{31}$$

where t is the incubation time in the protein solution

$$k_{ad} \approx \tau_{ad}^{-1} \exp\left(-\frac{V_{protein}}{\Sigma^{3/2}}\right) \tag{32}$$

and τ_{ad} is a characteristic microscopic time. The adsorbed area fraction after a time t is thus $\ln(1 - \theta) = -k_{ad}c_p t$. In turn, for $\theta \ll 1$ this reduces to $\theta \approx k_{ad}c_p t$. Accordingly, Γ values acquired with identical adsorption times will exhibit the $\ln N_{prim} \approx \text{const}' - V_{protein}/\Sigma^{3/2}$ behavior characterizing the equilibrium case. However, the irreversible adsorption scenario is associated with $\Gamma \sim t$ whereas experiments suggest that saturation is attained, thus supporting the equilibrium picture.

Acknowledgment. We acknowledge with thanks insightful discussions with A. Johner and M. Daoud.

LA701007J